MR Sept. 1944

NATIONAL ADVISORY COMMITTEE FOR AERONAUTICS

WARTIME REPORT

ORIGINALLY ISSUED
September 1944 as
Memorandum Report

TESTS OF A 0.30-SCALE SEMISPAN MODEL OF THE DOUGLAS XTB2D-1 AIRPLANE WING AND FUSELAGE COMBINATION IN THE NACA 19-FOOT PRESSURE TUNNEL

II - ROLL-FLAP POSITIONING AND LATERAL-CONTROL INVESTIGATION

By Stanley H. Spooner, C. Dixon Ashworth,
and Robert T. Russell

Langley Memorial Aeronautical Laboratory
Langley Field, Va.

WASHINGTON

NATIONAL ADVISORY COMMITTEE FOR AERONAUTICS

MEMORANDUM REPORT

for the

Bureau of Aeronautics, Navy Department

L-564

TESTS OF A 0.30-SCALE SEMISPAN MODEL OF THE DOUGLAS XTB2D-1 AIRPLANE WING AND FUSELAGE COMBINATION IN THE NACA 19-FOOT PRESSURE TUNNEL

II - ROLL-FLAP POSITIONING AND LATERAL-CONTROL INVESTIGATION

By Stanley H. Spooner, C. Dixon Ashworth, and Robert T. Russell

SUMMARY

Tests of a 0.30-scale semispan model of the Douglas XTB2D-1 airplane wing and fuselage combination equipped with full-span double-slotted flaps have been conducted in the NACA 19-foot pressure tunnel. This paper presents the results of that portion of the investigation concerning the development of the outboard flap, or roll flap. The purposes of these tests were (1) determination of the optimum relative positions of the wing, vane, and roll flap consistent with a high maximum lift coefficient and adequate rolling effectiveness; (2) determination of the roll-flap loads and hinge moments for design information; and (3) an estimation of the lateral-control forces of the airplane.

The results indicate that adequate rolling effectiveness and a high maximum lift coefficient may be obtained with the use of full-span double-slotted flaps. The lateral-control forces of the XTB2D-1 airplane meet the Navy Department requirements. However, it is recommended that the maximum value of the helix angle be raised by increasing the maximum roll-flap deflection for the flaps-retracted condition.

INTRODUCTION

At the request of the Bureau of Aeronautics, Navy Department, a 0.30-scale semispan model of the Douglas XTB2D-1 airplane wing and fuselage combination was tested in the NACA 19-foot pressure tunnel. The primary purposes of these tests were (1) to position the full-span double-slotted flaps so that adequate lateral control and a high maximum lift coefficient might be obtained; (2) to determine the effectiveness of the inboard flaps as a dive brake; and (3) to determine the full-span flap loads and hinge moments.

This report presents the results of the investigation to determine the optimum relative positions of the wing, vane, and roll flap, the roll-flap loads and hinge moments, and an estimation of the lateral-control characteristics of the airplane. The data and analysis of the other enumerated items are presented in reference 1.

A semispan model was tested for the purpose of securing data at a large Reynolds number. An end plate was installed in the tunnel to act as a reflection plane for maintaining the correct air flow and lift distribution over the wing.

COEFFICIENTS AND SYMBOLS

The coefficients and symbols used herein are defined as follows:

C_L lift coefficient (L/qS)

C_D drag coefficient (D/qS)

C_m pitching-moment coefficient ($M/qS\bar{c}$)

C_l rolling-moment coefficient (L'/qSb)

C_n yawing-moment coefficient (N/qSb)

C_{h_a} roll-flap hinge-moment coefficient $\left(H_a/qb_a\bar{c}_a^2\right)$

C_{N_a}	roll-flap normal-force coefficient (N_a/qS_a)
C_{C_a}	roll-flap chord force coefficient (C_a/qS_a)
C_{l_p}	rate of change of rolling-moment coefficient with helix angle $\left(\frac{\partial C_l}{\partial \frac{pb}{2V}}\right)$
P	pressure coefficient $\left(\frac{p - p_o}{q}\right)$

where

L	lift
D	drag
M	pitching moment
L'	rolling moment
N	yawing moment
H_a	roll-flap hinge moment measured about 0.262 roll-flap chord
N_a	roll-flap normal force
C_a	roll-flap chord force
$p - p_o$	difference between local static pressure and free-stream static pressure
q	dynamic pressure of free stream $\left(\frac{1}{2}\rho V^2\right)$
S	wing area (27.24 feet^2)
$\bar{c}$	mean aerodynamic chord (2.696 feet)
S_a	roll-flap area (2.654 feet^2)
pb/2V	helix angle, where p is the rolling velocity
b/2	model span (10.5 feet)
$b_a\bar{c}_a^2$	product of span and square of root-mean-square chord of roll flap (0.832 foot^3)

V	airspeed
V_i	indicated airspeed $\left(\sqrt{\frac{W/S}{0.001189C_L}}\right)$
ρ	mass density of air

and

α	corrected angle of attack of wing reference line
α'	tunnel angle of attack of wing reference line
δ_a	roll-flap deflection
δ_f	inboard flap deflection
δ_w	control wheel deflection
c_w	wing chord at any spanwise station
g_1	radial distance from wing lip to vane
l_1	distance, parallel to wing reference line, from wing lip to vane leading edge
g_2	radial distance from vane trailing edge to flap
l_2	distance, parallel to wing reference line, from vane trailing edge to flap leading edge
δ_{V_a}	roll-flap vane angle
δ_{c_a}	roll-flap cut-off angle
R	test Reynolds number ($\rho Vc/\mu$)
M	Mach number (V/a)
μ	coefficient of viscosity
a	sonic velocity
F_a	roll-flap control force at rim of wheel
r	control wheel radius (0.583 foot)
t	time

β angle of sideslip

ϕ angle of bank

MODEL AND TESTS

The general dimensions of the 0.30-scale XTB2D-1 semispan model and the arrangement of the model and the end plate in the 19-foot pressure tunnel are shown in figures 1 and 2. A complete description of the model is given in reference 1.

The tests were conducted with the air in the tunnel compressed to 35 pounds per square inch absolute pressure. For the majority of the tests, the dynamic pressure was approximately 50 pounds per square foot, corresponding to a test Reynolds number and a Mach number of approximately 5,200,000 and 0.12, respectively. The aerodynamic forces and moments were measured by an electrically recording, six-component balance system. The roll-flap loads and hinge moments were measured by means of resistance-type strain gages.

For vane and roll-flap positioning purposes, the roll flap was arbitrarily set at a deflection of 30°. The wing, vane, and roll-flap parameters (fig. 3) were measured relative to this position. The model was tested through a range of angles of attack and a range of roll-flap deflections for each of the roll-flap hinge-line and vane positions investigated. During this series of tests, excessive vibration of the roll flap at extreme deflections (48°) necessitated reducing the dynamic pressure to give a Reynolds number of approximately 4,300,000 for these high-deflection tests.

For the purpose of determining the lateral-control characteristics, the model was tested through an angle-of-attack range at several roll-flap deflections and at various extensions of the full-span flaps. For these tests the relative positions of the wing, vane, and roll flap at full extension were those determined from the positioning studies; these settings are shown in figure 4. The path of the roll flap and the vane from the retracted to the fully extended position is shown in figure 5. It should be noted that the attitude of the vane was fixed with respect to the wing for a given extension and was

not changed with a change in the roll-flap deflection. The attitude of the vane at other than full extension was determined from the linkage system intended for use on the airplane.

Since in the fully retracted position the roll flap deflected against the wing lip at positive deflections, roll-flap loads and hinge moments could not be determined. It was therefore necessary to allow a slight clearance between the roll flap and the wing lip and also to minimize the deflection by reducing the dynamic pressure to give a Reynolds number of approximately 4,300,000. The effects of the reduced dynamic pressure and of the clearance were not exactly determined but are believed to be small.

No tests of tab effectiveness were made.

Static-pressure tubes were installed flush with the upper and lower surfaces of the roll flap at a section approximately midspan of the roll flap in order to determine the pressure distribution for the retracted roll flap. Figure 6 gives a cross-sectional view of the roll flap showing the location of the pressure orifices. The pressure measurements were photographically recorded on a multiple-tube manometer.

The "standard model configuration" as used herein is defined as the plain wing and fuselage equipped with the small chord vanes and without the end-plate seal.

DATA AND CORRECTIONS

All results were reduced to standard nondimensional coefficients converted, with the exception of the rolling- and yawing-moment coefficients, so as to apply to a symmetrical complete wing and fuselage combination. The rolling- and yawing-moment coefficients apply to a complete wing and fuselage combination only for the condition where the left roll flap is deflected from neutral. The pitching, rolling, and yawing moments, as converted, are referred to the wind axes originating at the normal center-of-gravity location in the plane of symmetry at 25 percent of the mean aerodynamic chord and $0.032\bar{c}$ above the wing reference line.

Inasmuch as the desired results were primarily comparative, corrections were not applied for the effects of the drag and interference of the model support system. The effects are therefore included in the lift, drag, and pitching-moment coefficients. The increments in these coefficients are considered to be correct although the small increments in the tare values due to flap deflections are neglected.

However, corrections were applied for the effects of air-flow misalinement and jet boundary, which includes streamline curvature and the induced rolling and yawing moments due to the reflection plane. The value of the rolling moment recorded by the balance system with the roll flap in its neutral position was used as a tare, and the net rolling moment was thus equal to zero when the roll flap was set at neutral. This tare, then, may be considered as including practically all of the tare effects of the model support system on the rolling moments. The corrections applied to the yawing-moment coefficient were similar to those applied to the rolling-moment coefficient. Thus, the rolling- and yawing-moment coefficients may be considered to be absolute values. No corrections were applied to the roll-flap hinge-moment or force coefficients.

The magnitude and sign of the complete corrections to the gross data are given in the following equations:

$$C_D = C_{D_{gross}} + 0.012C_L^2$$

$$\alpha = \alpha' + 0.788C_L + 0.3$$

$$C_l = 0.900\left(C_{l_{gross}} - C_{l_{tare}}\right)$$

$$C_n = C_{n_{gross}} - C_{n_{tare}} - 0.0314C_{l_{corr}}C_{L_{gross}}$$

RESULTS AND DISCUSSION

Positioning Investigation

The lift and rolling characteristics for the various relative positions of the wing lip, vane, and roll flap are shown in figure 7. A cross plot of figure 7, giving rolling-moment coefficient with respect to roll-flap deflection for an angle of attack of 9°, is shown in figure 8 from which the effects of the roll-flap parameters may be observed.

It should be noted here that the lift coefficients of figure 7 actually represent values which would be obtained on a full-span model with both roll flaps deflected equally in the same direction. Any estimate of roll-flap characteristics for specified lift coefficients should therefore be made using the lift coefficient obtained with the roll flap in its neutral position.

The effects of the various roll-flap parameters on the rolling effectiveness at large roll-flap deflection may be summarized in the following table, prepared from the data of figures 7 and 8:

Roll-flap arrangement	δ_{V_a} (deg)	g_1/c_w	l_1/c_w	g_2/c_w	l_2/c_w	δ_{c_a} (deg)	C_l for $\delta_a = 48°$ ($\Delta\delta_a = 18°$)	$C_{L_{max}}$ ($\delta_a = 30°$)
1	44	0.019	0.011	0.017	0.048	38	0.0162	2.69
2	40	.019	.011	.017	.048	38	.0266	2.71
3	40	.015	.011	.022	.048	38	.0295	2.72
4	40	.015	.011	.017	.048	38	.0270	2.75
5	40	.015	.011	.017	.048	31	.0290	2.67
6	34	.015	.011	.017	.048	38	.0303	2.67
7	40	.015	.014	.012	.048	38	.0160	2.74
8	40	.015	.011	.017	.052	38	.0280	2.77

As shown by the values in the preceding table, arrangement 6 gave the best rolling effectiveness for large deflections while still providing a reasonably

high maximum lift coefficient for neutral roll flap ($\delta_a = 30^\circ$). Because of undesirable roll-flap vibration observed in tests of this combination, however, it was decided that arrangement 3 was the most satisfactory of the combinations tested. These settings were selected as the optimum arrangement and used in the remainder of the lateral-control investigation.

The effectiveness of the roll flap appears to be sensitive to small changes in the vane angle δ_{V_a} and also to small variations in the vane-roll-flap gap g_2, although the results are not conclusive in the case of the latter parameter. In the range tested, the effectiveness of the roll flap is only slightly affected by small changes in the other parameters.

Lateral-Control Characteristics

In figures 9 through 15 the characteristics of the model and the roll flap for the retracted, intermediate, and fully extended positions of the full-span flaps are presented for several angles of attack. A smooth variation of rolling velocity with roll-flap deflection is indicated. The data in these figures were cross-plotted from the original data, a representative plot of which is shown in figure 16. The lift, drag, and pitching-moment characteristics of the model for the neutral roll-flap deflections at the various extensions are given in figure 17. The data obtained from tests of the XTB2D-1 semispan model are analyzed herein to give estimated full-scale values of the helix angle and the wheel forces.

Flaps neutral.- The value of the helix angle for the flaps-retracted flight conditions is estimated as

$$\frac{pb}{2V} = \frac{0.8C_l}{C_{l_p}}$$

where the value $C_{l_p} = 0.57$ was obtained by correcting the value indicated in reference 2 to a lift-curve slope of 0.108 rather than the theoretical lift-curve slope of 0.099 used in reference 2. The factor 0.8 is empirically determined from attempts to correlate wind-tunnel and

flight data and allows for reductions in the available rolling moment due to adverse yaw at low speeds and to wing twisting and compressibility at high speeds. The wheel forces in steady rolls were determined from the following equation:

$$F_a = \frac{qb_a\bar{c}_a^2}{r}\left[-\frac{C_{h_{a_{up}}}}{\left(\frac{d\delta_w}{d\delta_a}\right)_{up}} - \frac{C_{h_{a_{down}}}}{\left(\frac{d\delta_w}{d\delta_a}\right)_{down}}\right]$$

where the hinge-moment coefficients were corrected for the change in local effective angle of attack due to steady rolling. The mechanical advantage of the control system which was used in the determination of the wheel forces is given in figure 18.

The estimated roll-flap effectiveness for the flaps-retracted condition is shown in figure 19. The conditions considered correspond to 120 and 140 percent of the flaps-retracted stalling speed and to 80 percent of the expected maximum speed. The stalling speeds were determined using an assumed wing loading of 39.7 pounds per square foot and values of maximum lift coefficient determined from reference 1. A maximum speed of 303 miles per hour indicated was assumed on the basis of information supplied by the contractor. At 80 percent of the maximum speed, a wheel force of 78 pounds is required to produce a wing-tip helix angle of 0.070 radian at the maximum roll-flap deflection. The Navy Department requirements as specified in reference 3 state that the lateral-control device should be of sufficient power to give a wing-tip helix angle equal to or greater than 0.08 and that at any speed above 140 percent of the stalling speed and below 80 percent of the maximum speed the wheel force shall not exceed 80 pounds. In order to meet the requirement that the helix angle $pb/2V$ be equal to or greater than 0.08, it appears that more roll-flap deflection is necessary. The variation of control force with helix angle appears smooth.

Flaps deflected.- The 0.8 factor used in the determination of the wing-tip helix angles was based upon a comparison of flight and wind-tunnel tests of conventional aileron arrangements for which the ratio of the adverse

yawing moment to rolling moment was of the order of -0.2. In the present tests, with the full-span flaps deflected 30°, the ratio was approximately -0.33 at 120 percent of the stalling speed. Moreover, the adverse yaw due to rolling is greater with full-span flaps than with partial-span flaps or no flaps. For these reasons it was felt that the 0.8 factor was not applicable to the full-span-flap case. Using lateral-stability derivatives and mass characteristics supplied by the Douglas Company on the basis of complete model tests and design data, the motions of the airplane following abrupt full roll-flap deflection were calculated by the methods of reference 4. The results of these calculations are shown in figures 20 and 21. Although the present tests were made with flaps deflected 30°, the stability derivatives were estimated for the airplane in its actual flight configuration in which the outboard flap deflection was approximately 20° and the inboard flap deflection approximately 36° at the speed considered (92 miles per hour indicated). The quantitative results of figures 20 and 21, therefore, will not apply exactly to either configuration. It is believed, however, that the curves may be accepted as a reasonable indication of the motions of the airplane in its flight configuration at a speed slightly above 120 percent of the stalling speed.

No rolling reversal is observed but the rolling velocity is noticeably reduced by the adverse yaw. The curves of figure 21 indicate that an arbitrary value of $\frac{pb}{2V} = \frac{0.6C_l}{C_{l_p}}$ $\left(\text{rather than } \frac{0.8C_l}{C_{l_p}}\right)$ would be in fair agreement with the calculated rolling motion. This lower factor was used in estimating over-all average values of pb/2V for use in calculating the aileron control forces which are shown plotted against average helix angle in figure 22. For full deflection, average pb/2V values in excess of 0.08 are indicated, with satisfactorily low control forces. Variation of control force with helix angle appears smooth.

Inasmuch as the rolling velocity did not remain constant with time, it was thought desirable to present values of effective pb/2V during periods of time required to reach certain angles of bank. These values are shown in figure 23.

It may be noted that the maximum angle of sideslip shown in figure 20 is approximately 35° - considerably higher than the ordinarily accepted maximum of 20°. No computations, however, were made to determine the amounts of rudder deflection or pedal force required to counteract the sideslip.

Roll-flap pressure distribution.- The chordwise pressure distribution over the retracted roll flap is presented in figure 24. The pressure distribution is given for several roll-flap deflections and for various angles of attack of the model. An insufficient number of pressure orifices in the vicinity of the wing lip prevented the determination of the peak pressures. Consequently, the pressure diagrams are not closed. The trends, however, are indicated by arrows.

CONCLUSIONS

On the basis of the XTB2D-1 semispan model test data presented herein, the following conclusions may be drawn:

1. Adequate rolling effectiveness and a high maximum lift coefficient were obtained with full-span double-slotted flaps deflected for values of the roll-flap parameters as follows:

Vane angle, deg	40
Lip-vane gap	$0.015c_w$
Lip-vane overhang	$0.011c_w$
Vane-roll-flap gap	$0.022c_w$
Vane-roll-flap overhang	$0.048c_w$
Cut-off angle, deg	38

2. Roll-flap effectiveness appears to be sensitive to small variations of the vane angle. The effects of the vane-roll-flap gap cannot be isolated completely, but small changes in the value of this parameter appear to influence the roll-flap effectiveness appreciably. The remaining parameters appear to have little effect in the range investigated.

3. The estimated maximum helix angle and the corresponding wheel force are 0.070 radian and 78 pounds,

respectively, for the 80-percent maximum speed, flaps-up condition. Helix angles up to 0.081, with small wheel forces, are estimated for the low-speed flaps-extended condition.

4. It is recommended that the maximum roll-flap deflection for the flaps-retracted condition be increased in order to obtain a $pb/2V$ of 0.08 as required by the Navy Department specifications.

Langley Memorial Aeronautical Laboratory
National Advisory Committee for Aeronautics
Langley Field, Va., September 7, 1944

REFERENCES

1. Ashworth, C. Dixon, Spooner, Stanley H., and Russell, Robert T.: Tests of a 0.30-Scale Semispan Model of the Douglas XTB2D-1 Airplane Wing and Fuselage Combination in the NACA 19-Foot Pressure Tunnel. I - Full-Span Flap and Air-Brake Investigation. NACA MR, Sept. 7, 1944.

2. Pearson, Henry A., and Jones, Robert T.: Theoretical Stability and Control Characteristics of Wings with Various Amounts of Taper and Twist. NACA Rep. No. 635, 1938.

3. Anon.: Specification for Stability and Control Characteristics of Airplanes. SR-119, Bur. Aero., Oct. 1, 1942.

4. Jones, Robert T.: A Simplified Application of the Method of Operators to the Calculation of Disturbed Motions of an Airplane. NACA Rep. No. 560, 1936.

TABLE I.- INDEX OF FIGURES

Figure	Presentation	Plot	Percent full-span flap extension	δ_f (deg)	δ_a (deg)
1	Three-view drawing of model	----------	----------	-----	-----
2	View of model in tunnel	----------	----------	-----	-----
3	Roll-flap parameters	----------	100	-----	30
4	Optimum roll-flap and vane position	----------	100	-----	30
5	Roll-flap extension path	----------	----------	-----	-----
6	Location of roll-flap pressure orifices	----------	----------	-----	-----
7	Roll-flap positioning	C_l, α vs C_L	100	55	Vary
8	Summary of fig. 7	δ_a vs C_l	100	55	Do.
9	Roll-flap characteristics	C_l, C_{h_a}, C_n, C_{N_a}, C_{C_a} vs δ_a	0	0	Do.
10	----------do----------	------do------	0	11	Do.
11	----------do----------	------do------	30	0	Do.
12	----------do----------	------do------	50	0	Do.
13	----------do----------	------do------	70	7	Do.
14	----------do----------	------do------	100	7	Do.
15	----------do----------	------do------	100	30	Do.
16	----------do----------	C_l, C_{h_a}, C_n, C_{N_a}, C_{C_a} vs α	0	0	Do.

TABLE I.- INDEX OF FIGURES - Concluded

Figure	Presentation	Plot	Percent full-span flap extension	δ_f (deg)	δ_a (deg)
17	Aerodynamic characteristics	α, C_D, C_m vs C_L	Vary	Vary	Vary
18	Roll-flap control linkage	δ_a vs δ_w	0, 100	0,30	Do.
19	Full-scale roll-flap effectiveness	F_a vs pb/2V	0	0	----
20	Time history of airplane	ϕ,β, p vs t	100	30	----
21	Bank characteristics	ϕ vs t	100	30	Vary
22	Full-scale roll-flap effectiveness	F_a vs pb/2V	100	30	----
23	Effective pb/2V to roll to various angles of bank	pb/2V vs ϕ	100	30	----
24	Roll-flap pressure distribution	P vs percent roll-flap chord	0	0	Vary

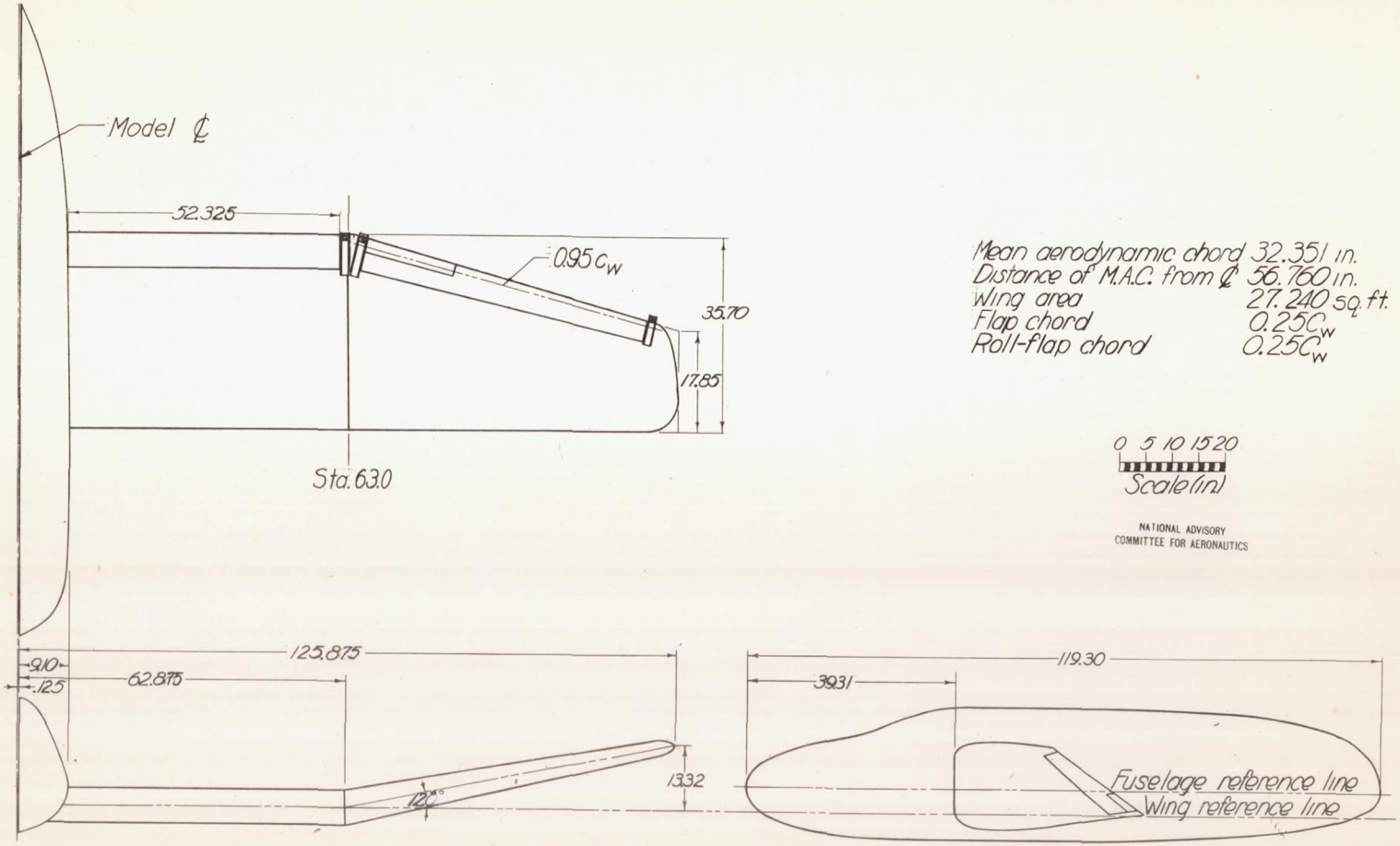

Figure 1.- Three-view drawing of the 0.30-scale semispan model of the Douglas XTB2D-1 Airplane.

L-564

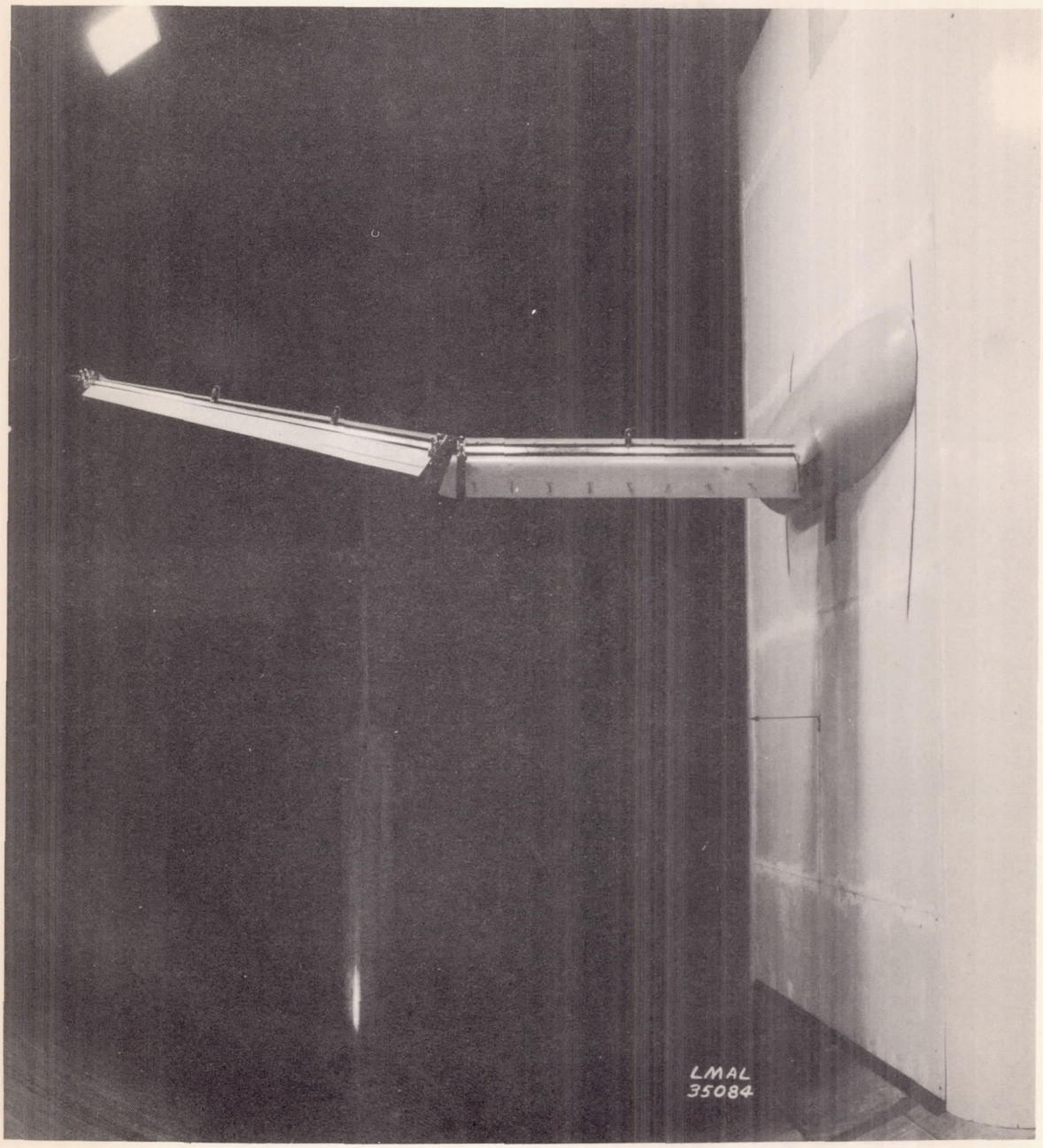

Figure 2.- View of the 0.30-scale semispan model of the Douglas XTB2D-1 airplane mounted in the 19-foot pressure tunnel.

NATIONAL ADVISORY COMMITTEE FOR AERONAUTICS
LANGLEY MEMORIAL AERONAUTICAL LABORATORY - LANGLEY FIELD, VA.

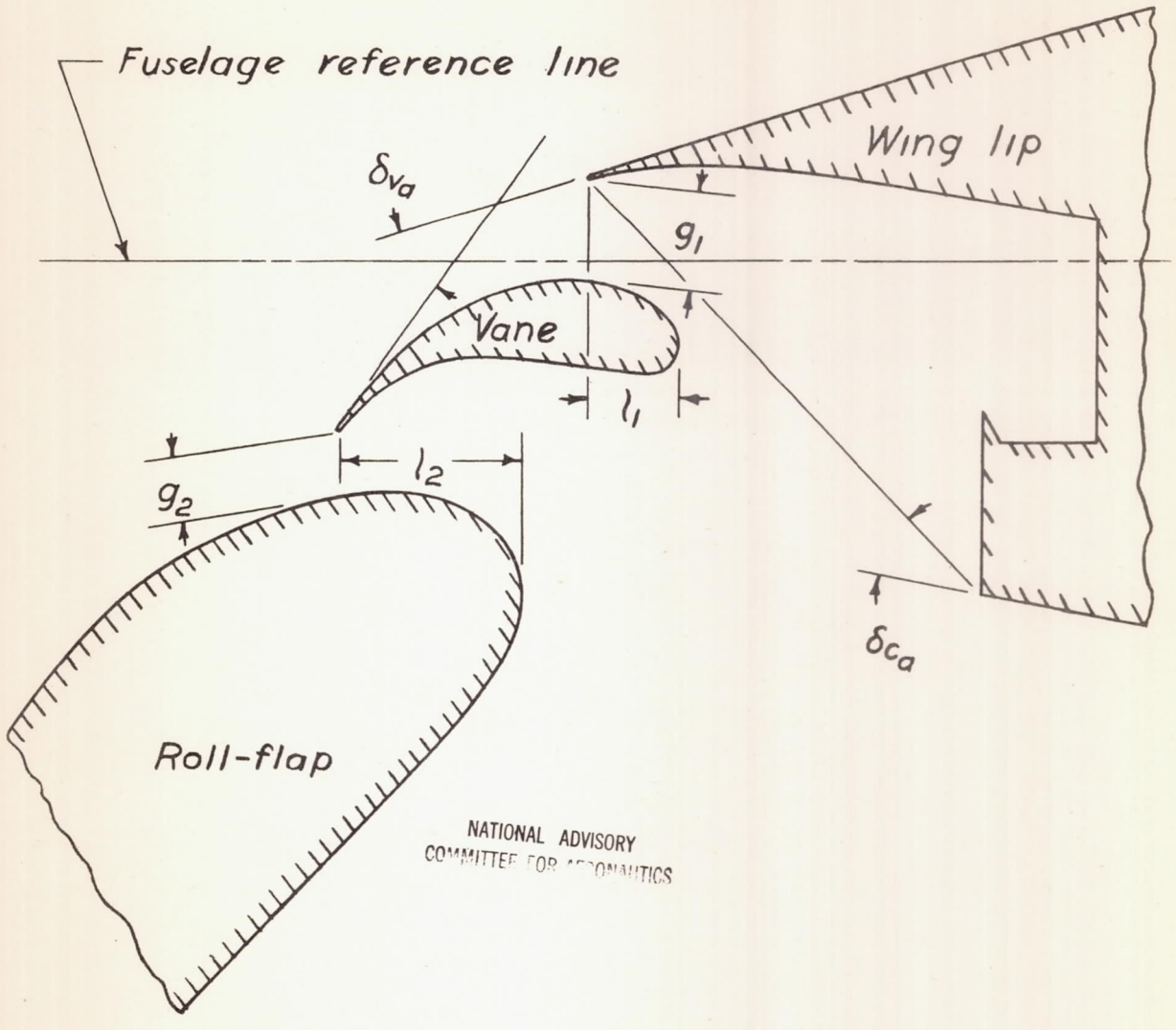

Figure 3.-Roll-flap parameters.

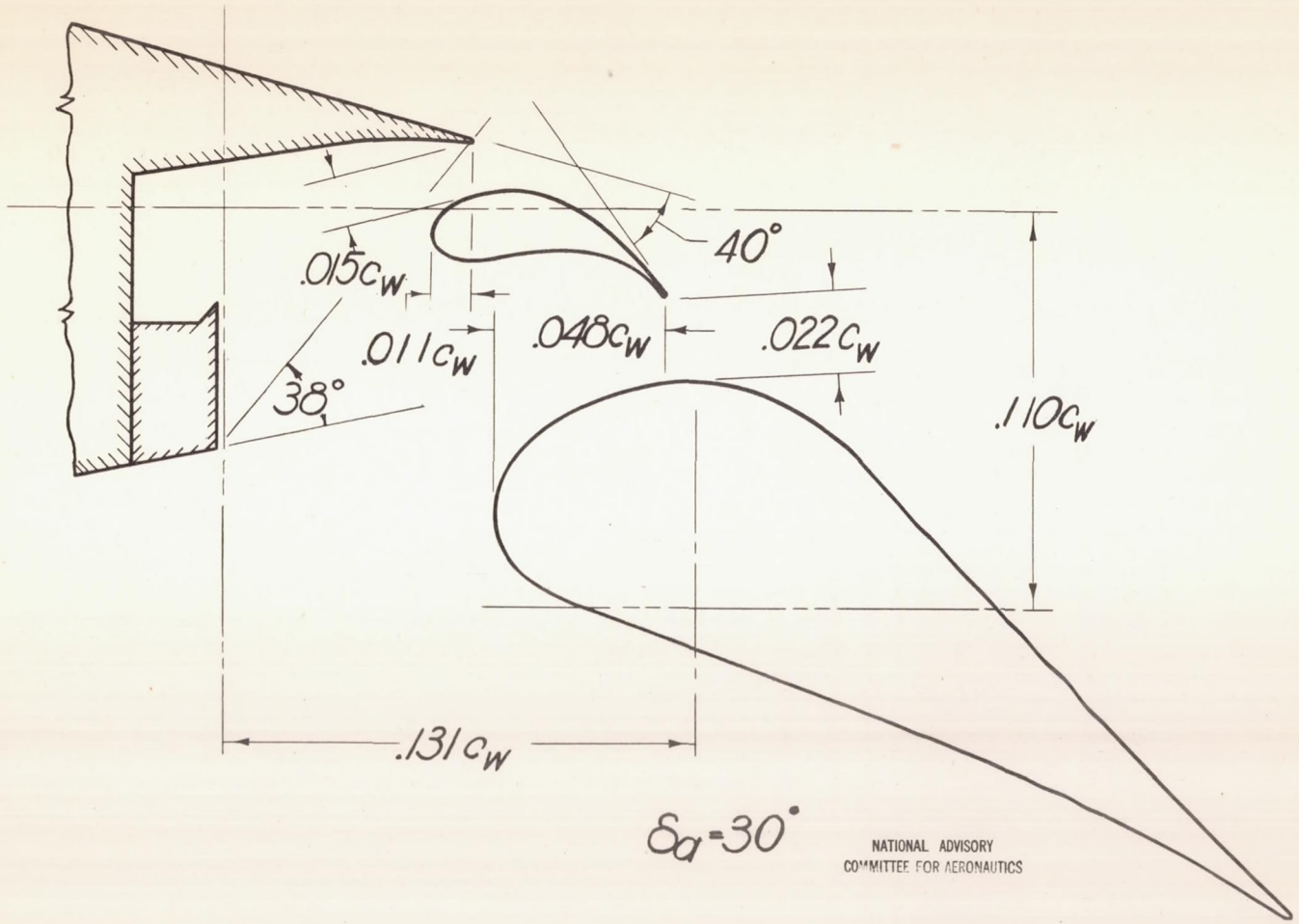

Figure 4.- Relative location of wing, vane, and roll-flap at full extension.

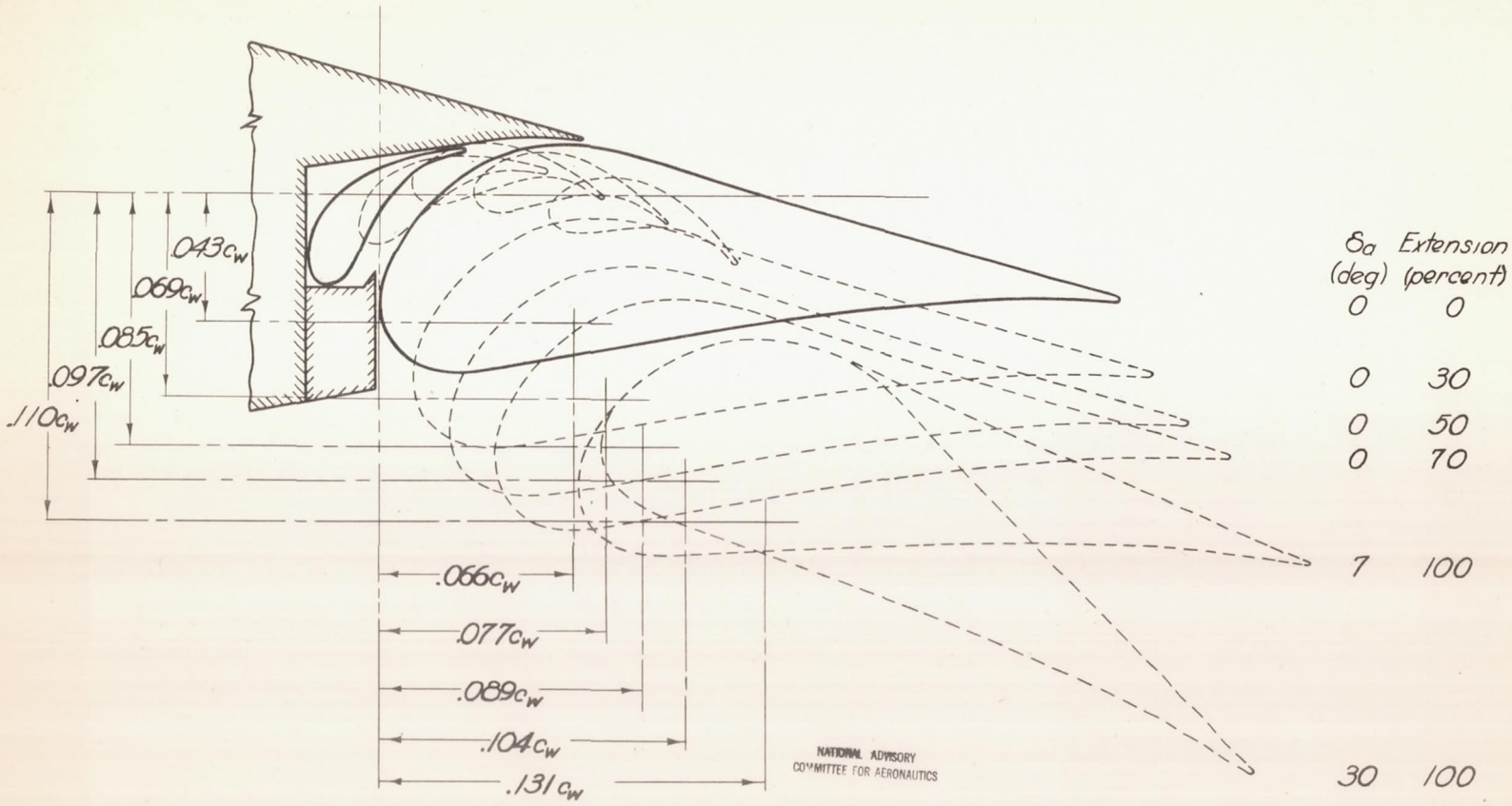

Figure 5.- Roll-flap and vane position at various extensions.

L-564

UPPER SURFACE	
Orifice Tube No.	Tube Location Percent of chord
14	6.2
13	34.6
12	48.2
11	66.5
10	84.6

LOWER SURFACE	
Orifice Tube No.	Tube Location Percent of chord
1	0.2
2	1.9
3	4.7
4	7.8
5	11.9
6	17.8
7	48.3
8	69.1
9	89.9

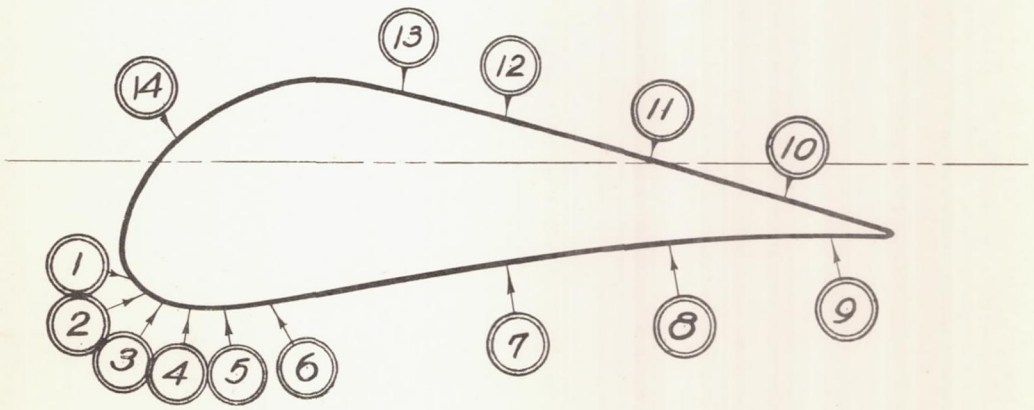

Figure 6. — Chordwise location of roll-flap pressure orifices.

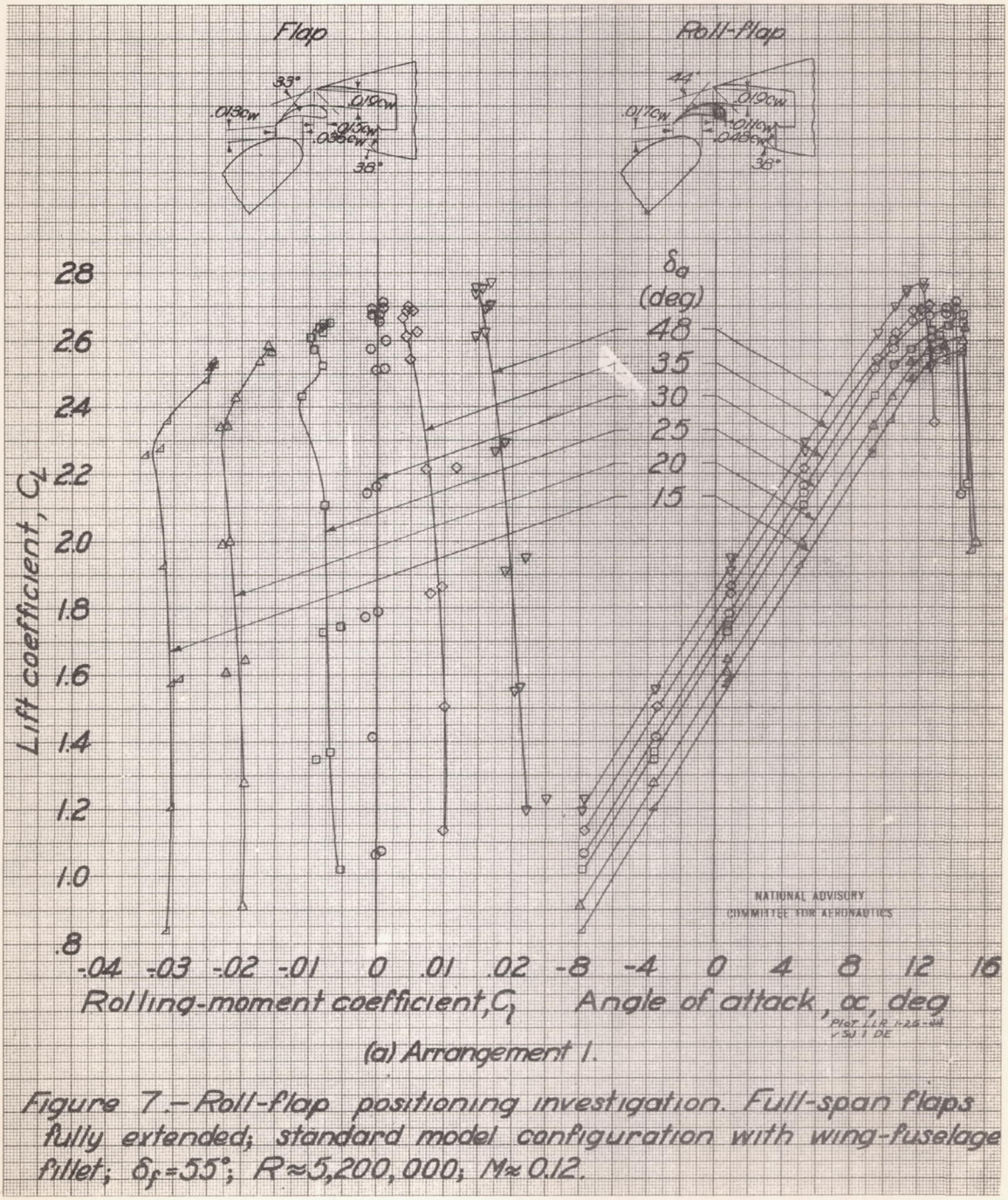

(a) Arrangement 1.

Figure 7.– Roll-flap positioning investigation. Full-span flaps fully extended; standard model configuration with wing-fuselage fillet; $\delta_f = 55°$; $R \approx 5{,}200{,}000$; $M \approx 0.12$.

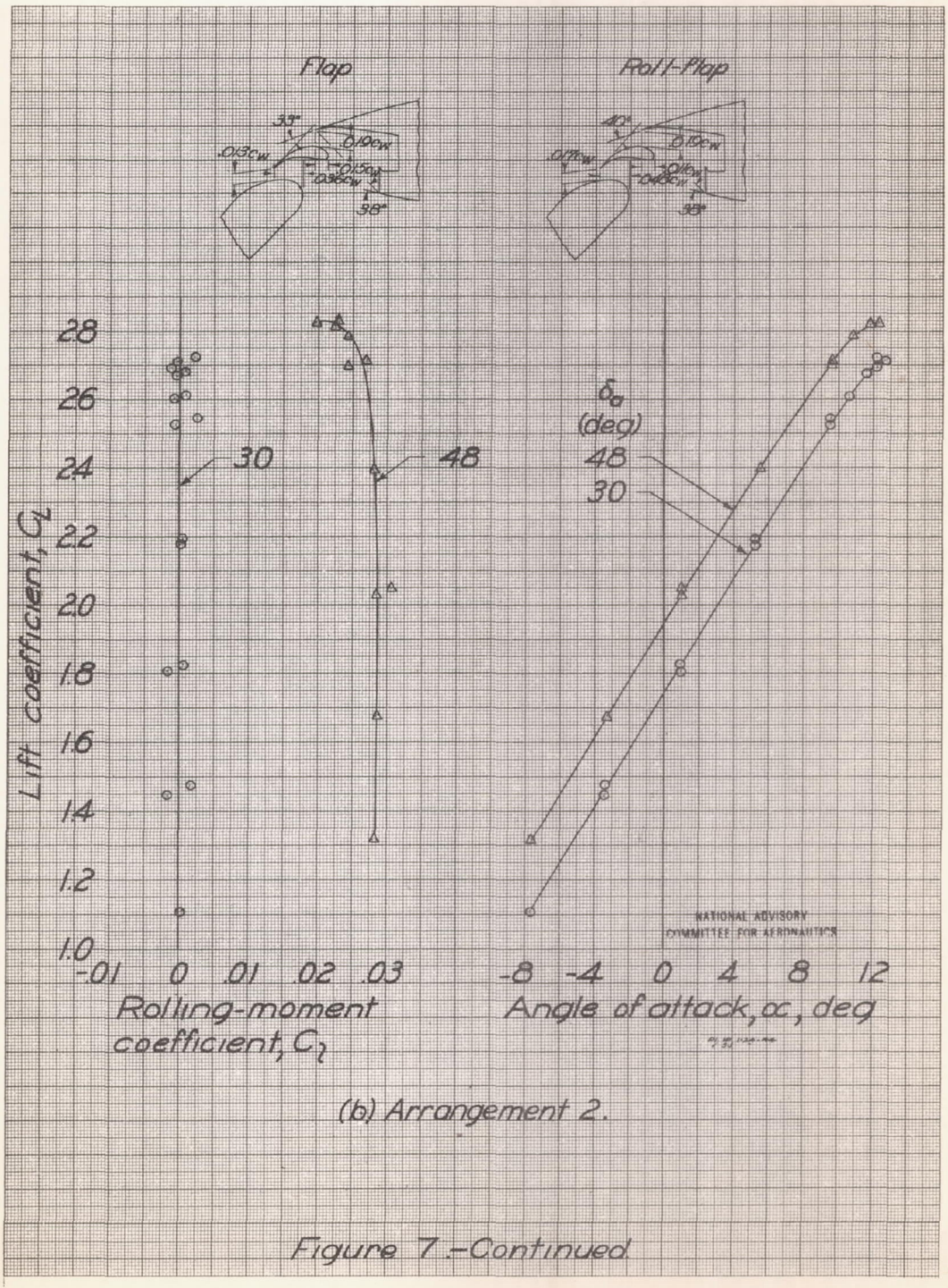

(b) Arrangement 2.

Figure 7.–Continued

L-564

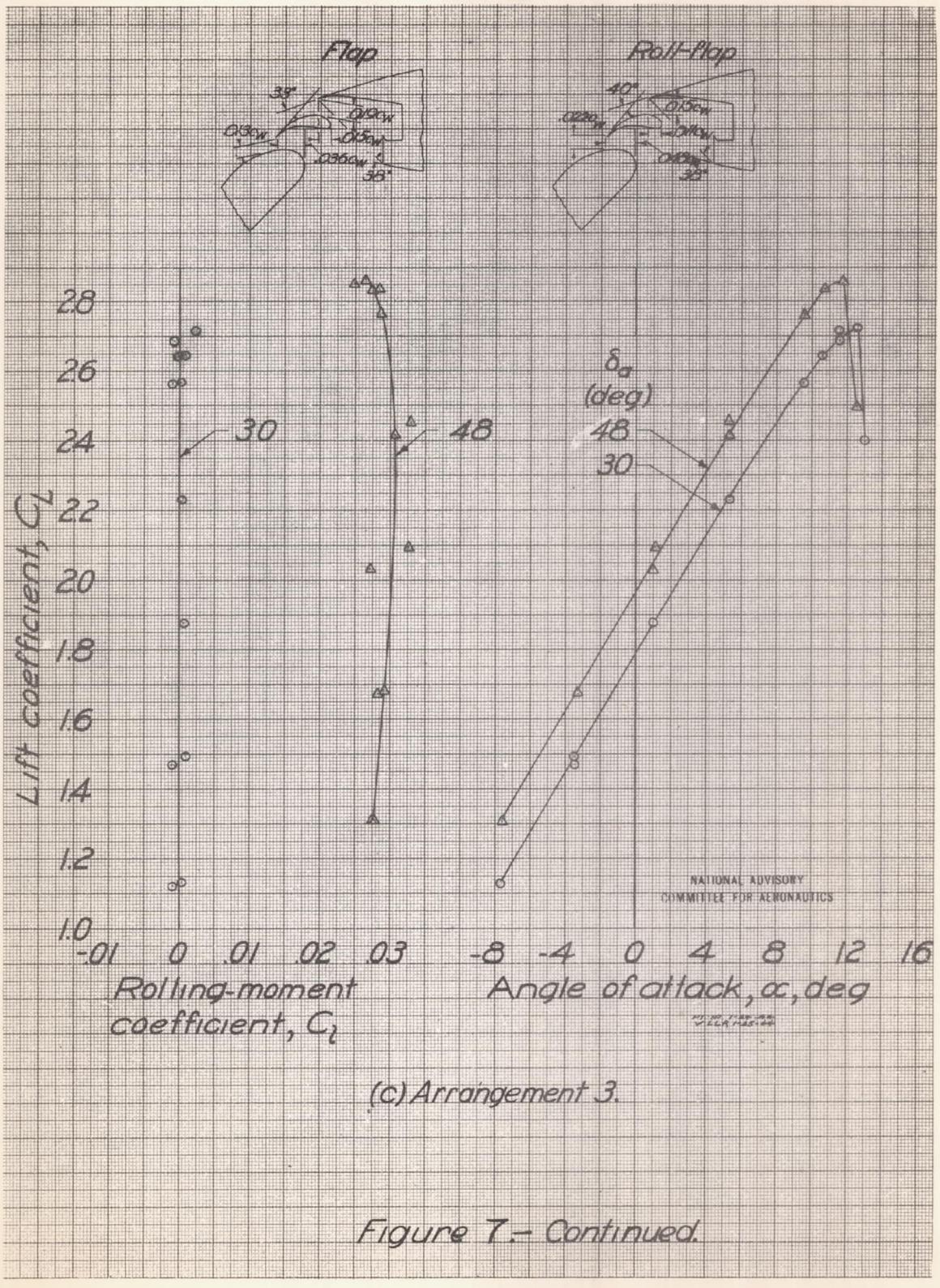

(c) Arrangement 3.

Figure 7.- Continued.

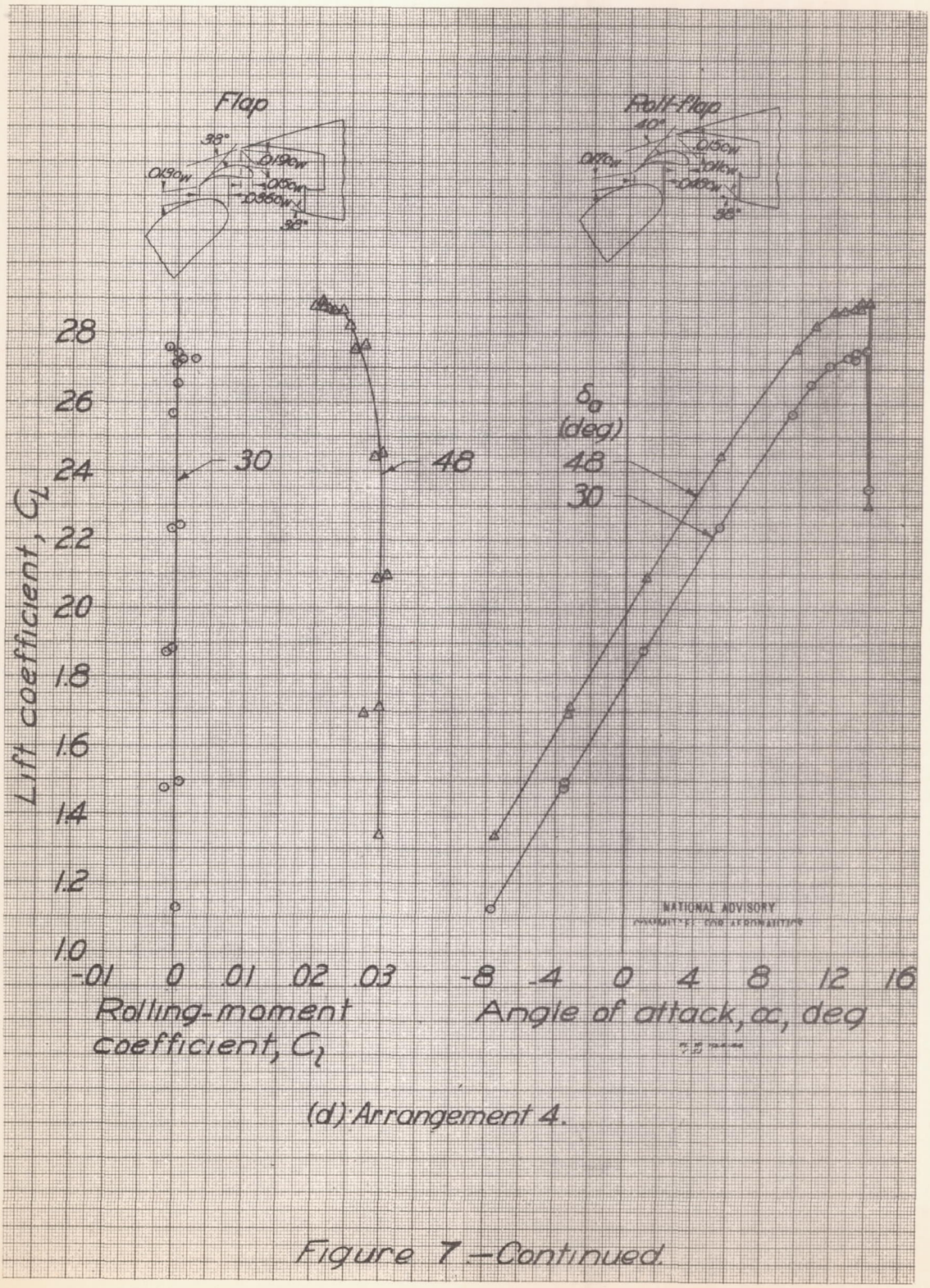

(d) Arrangement 4.

Figure 7.—Continued.

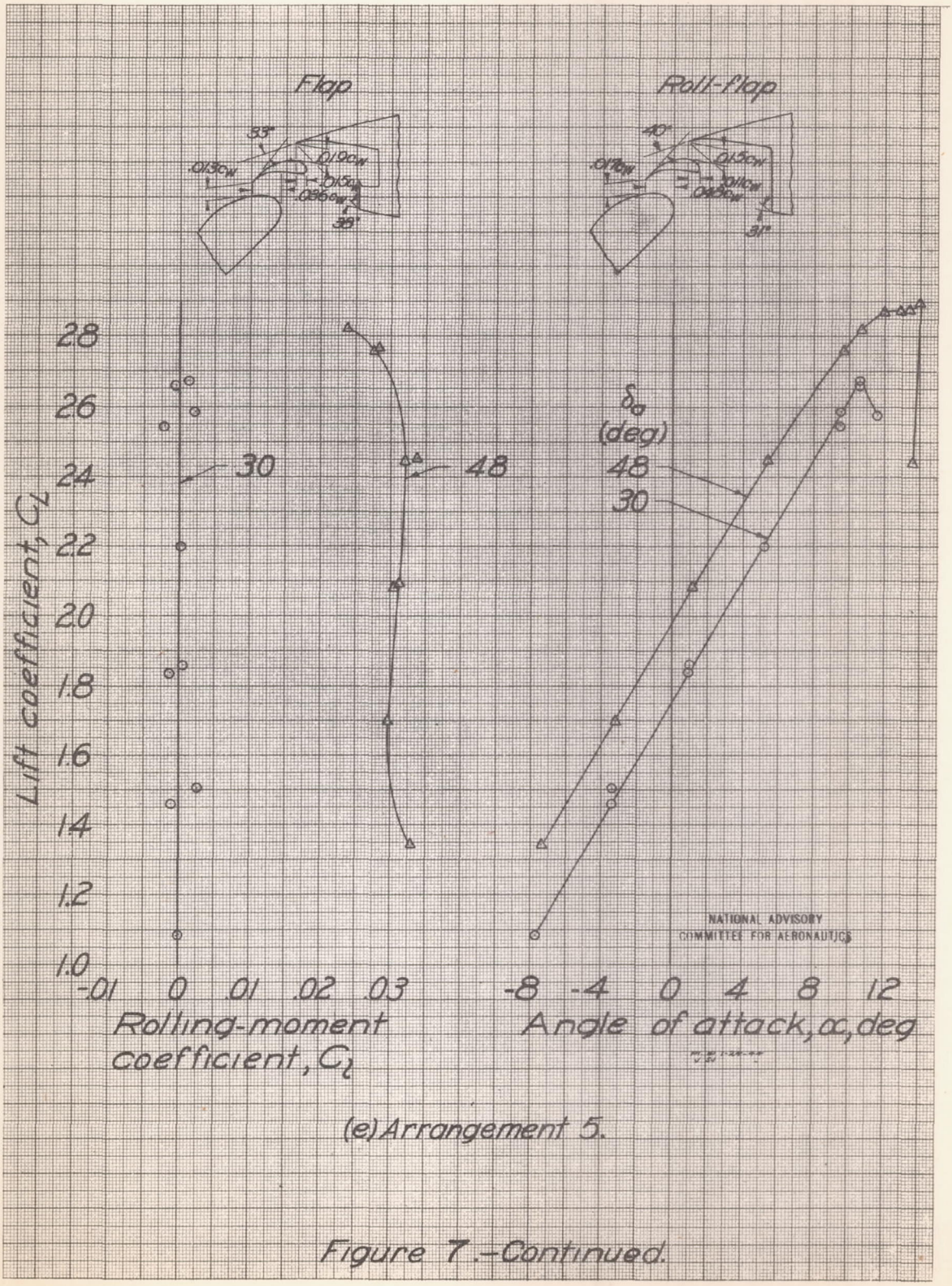

(e) Arrangement 5.

Figure 7.—Continued.

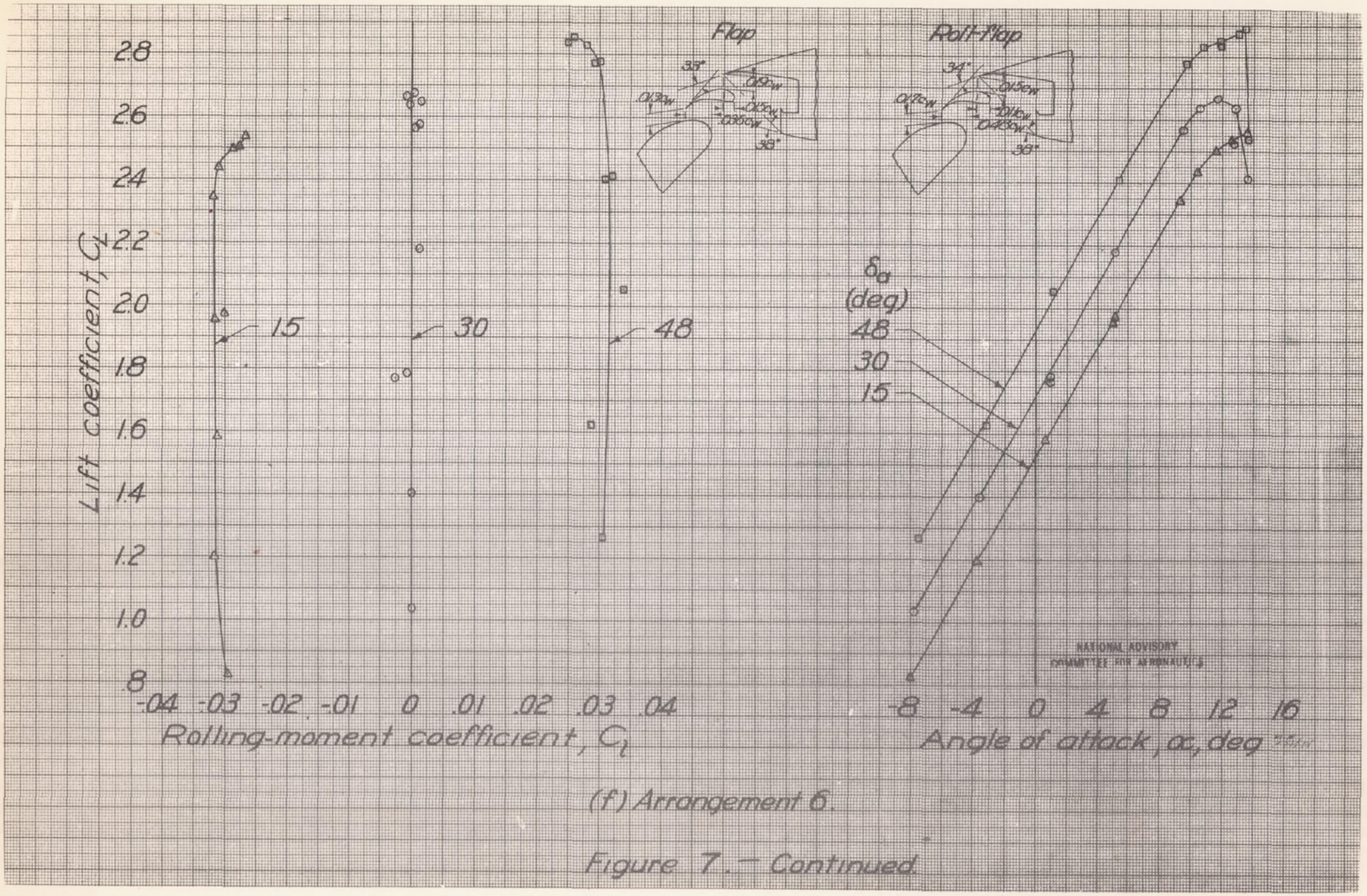

(f) Arrangement 6.

Figure 7.- Continued.

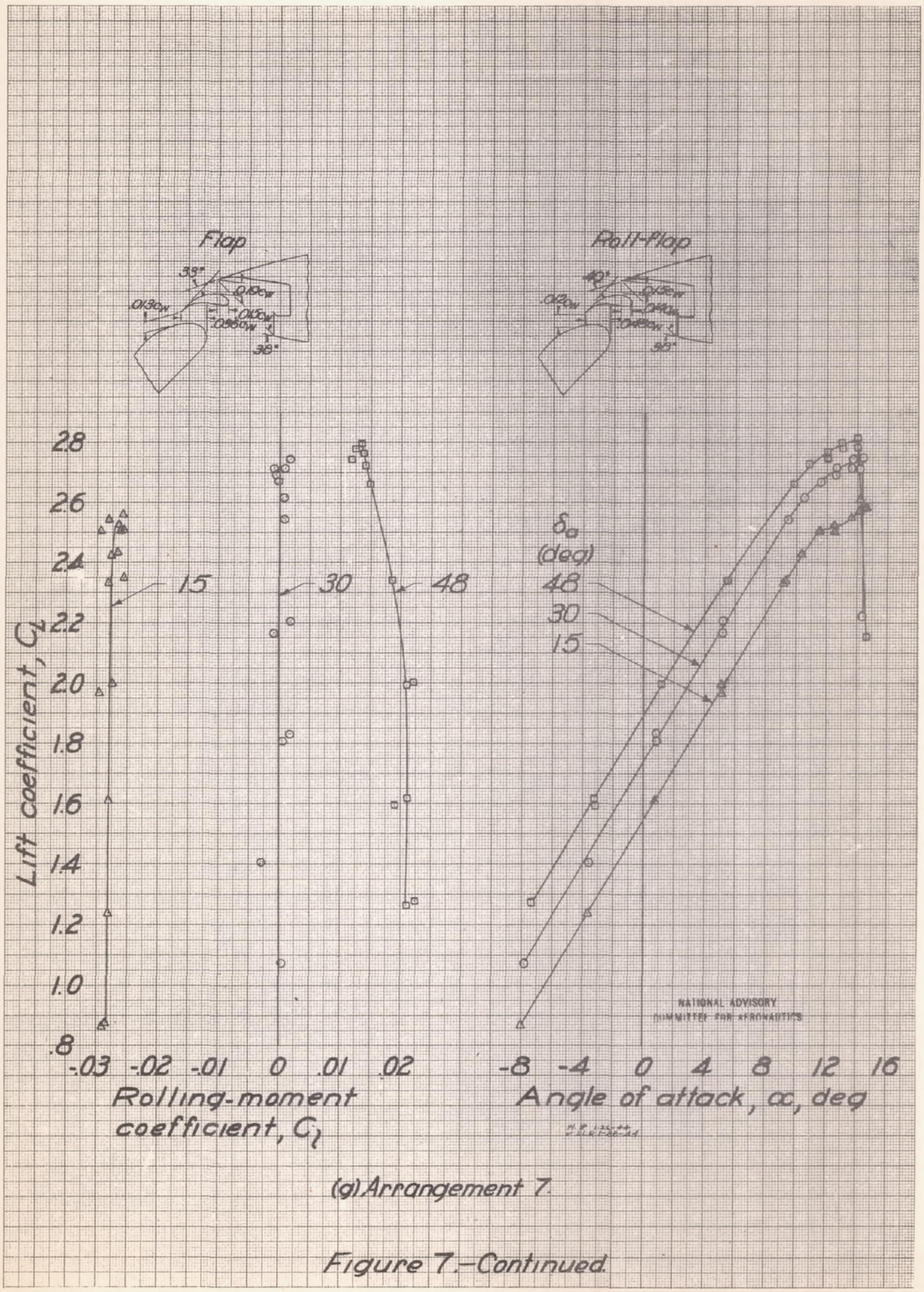

(g) Arrangement 7.

Figure 7.—Continued.

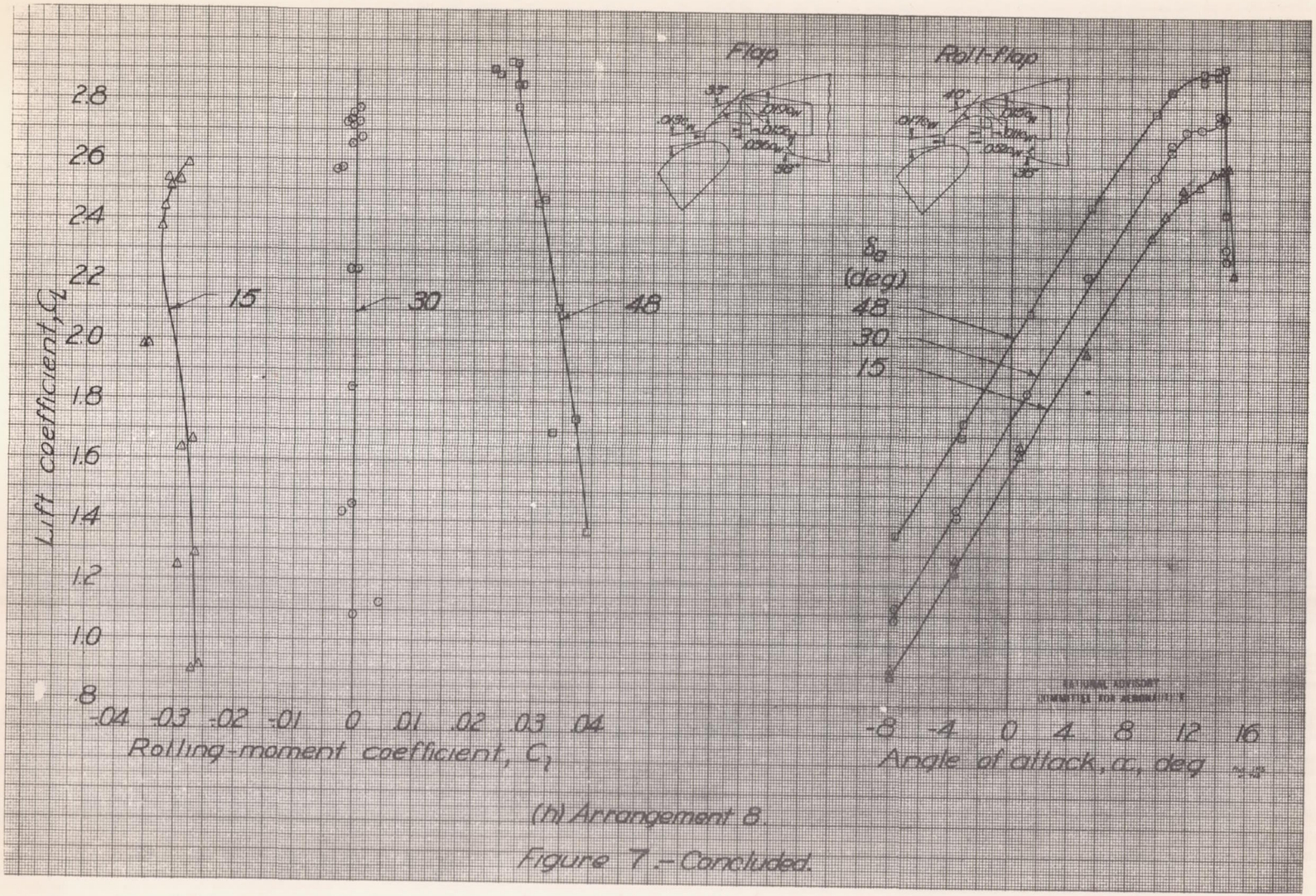

(h) Arrangement 8.

Figure 7.- Concluded.

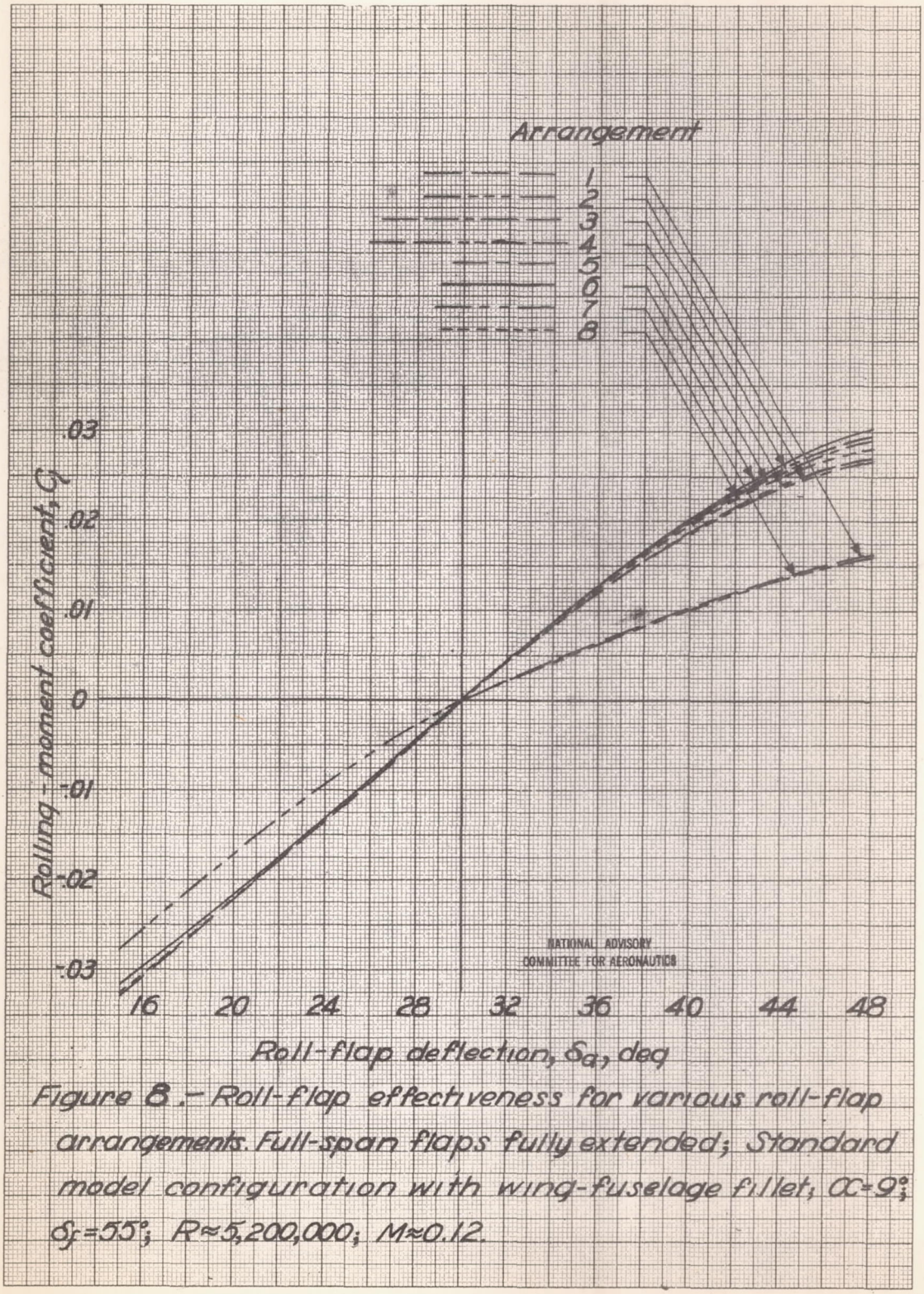

Figure 8.- Roll-flap effectiveness for various roll-flap arrangements. Full-span flaps fully extended; Standard model configuration with wing-fuselage fillet, $\alpha = 9°$; $\delta_f = 55°$; $R \approx 5{,}200{,}000$; $M \approx 0.12$.

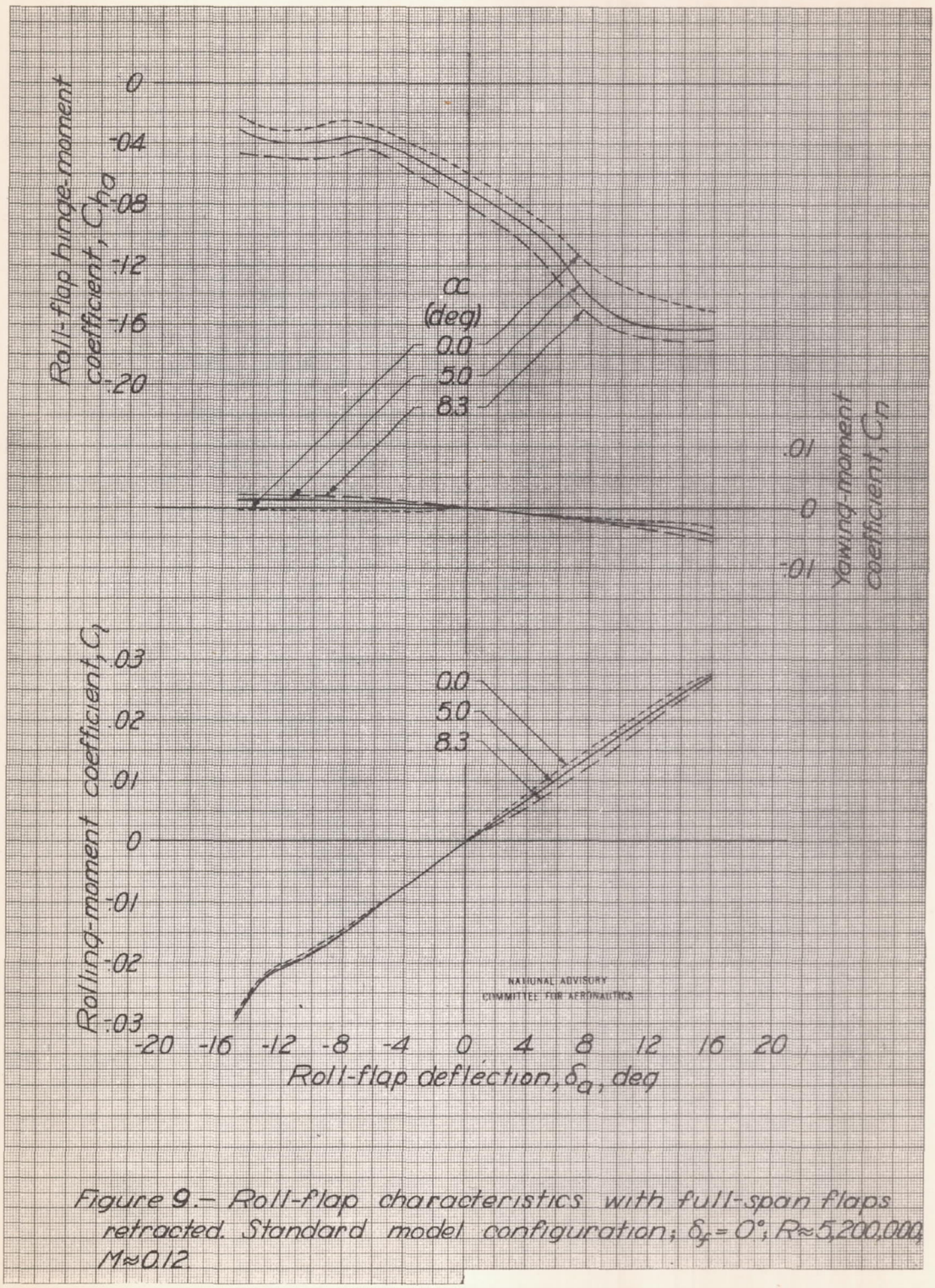

Figure 9.– Roll-flap characteristics with full-span flaps retracted. Standard model configuration; $\delta_f = 0°$; $R \approx 5{,}200{,}000$, $M \approx 0.12$

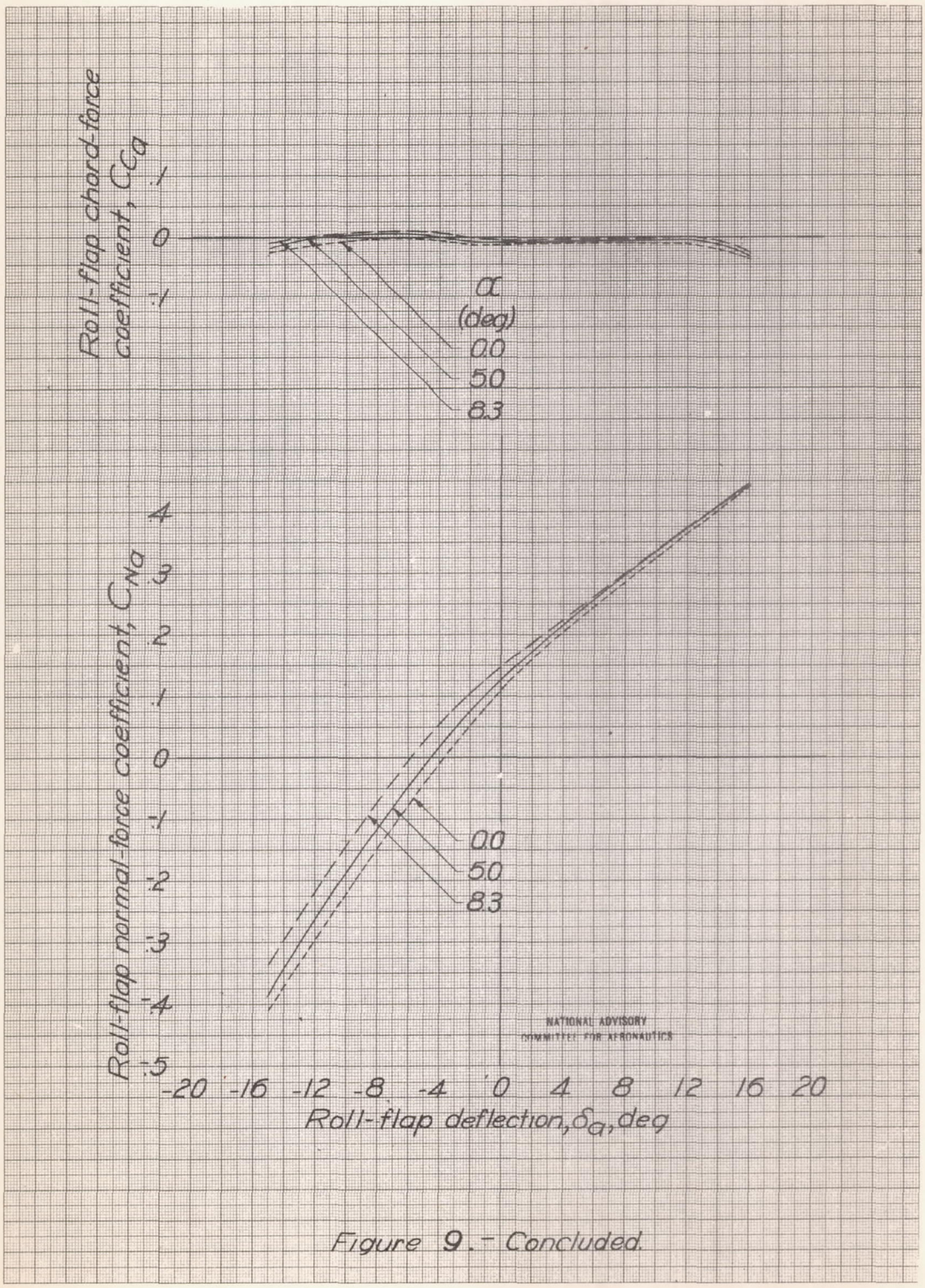

Figure 9.- Concluded.

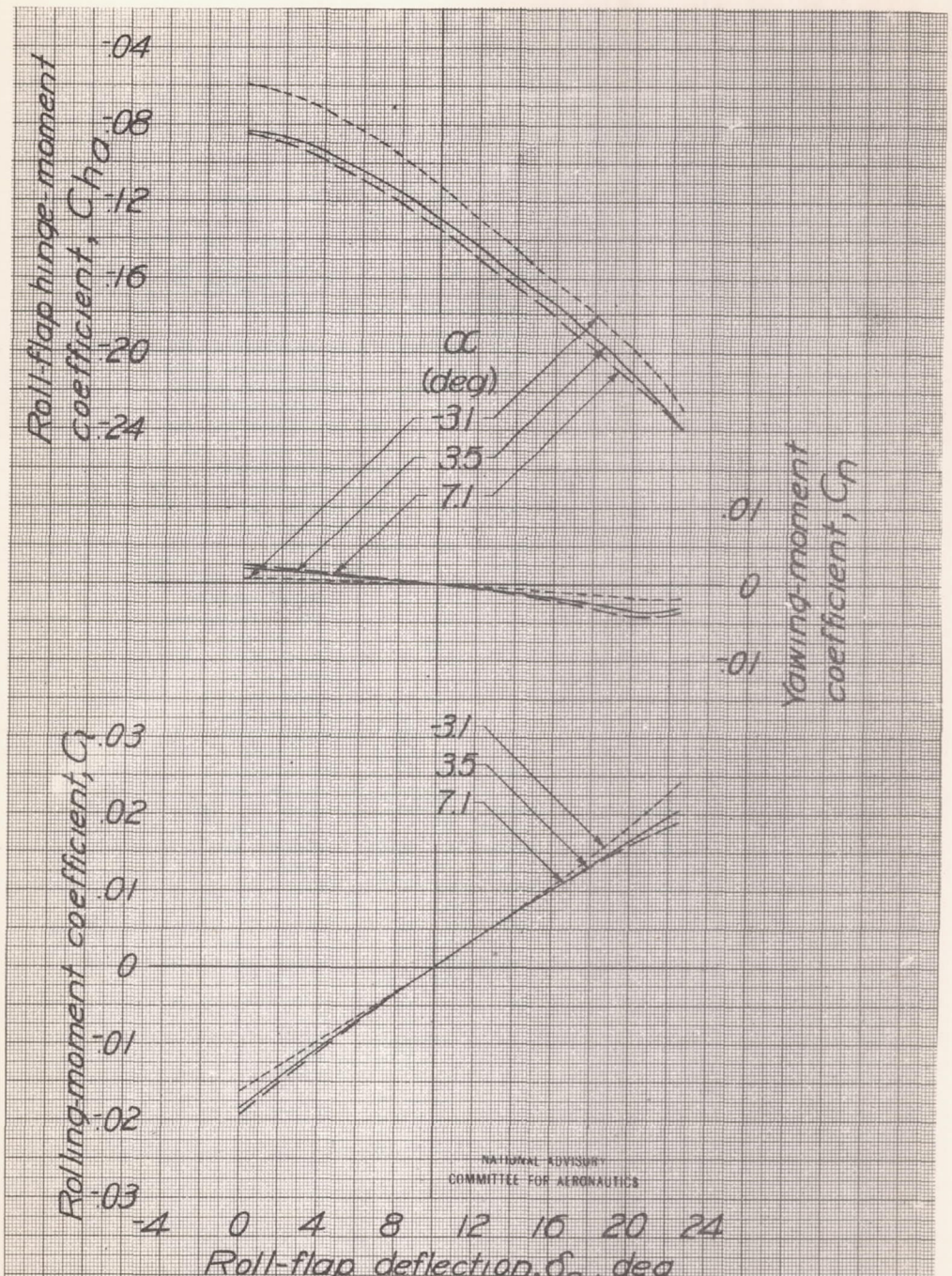

Figure 10.– Roll-flap characteristics with full-span flaps retracted. Standard model configuration; $\delta_f = 11°$; $R \approx 4{,}800{,}000$; $M \approx 0.11$.

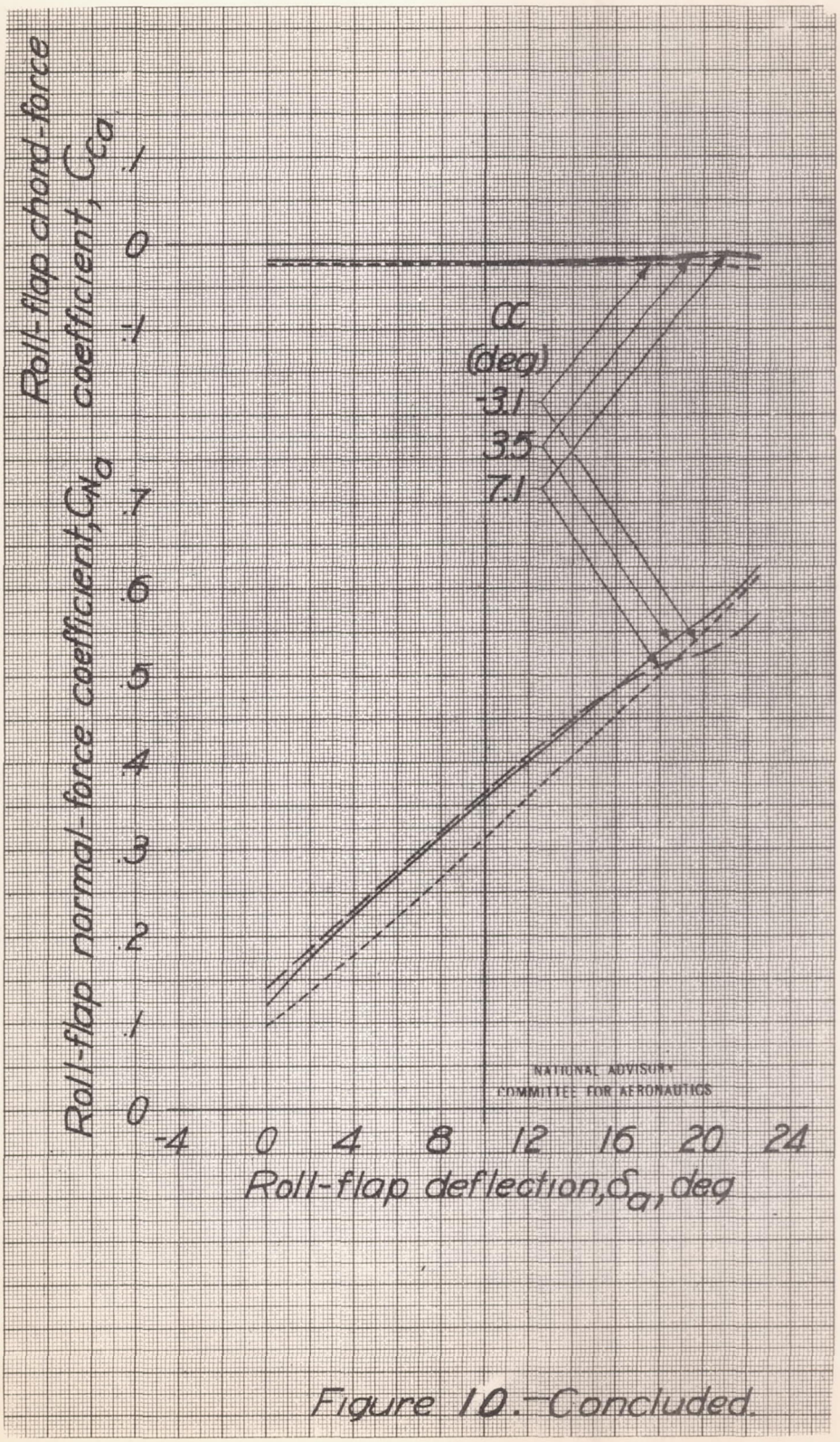

Figure 10.—Concluded.

L-564

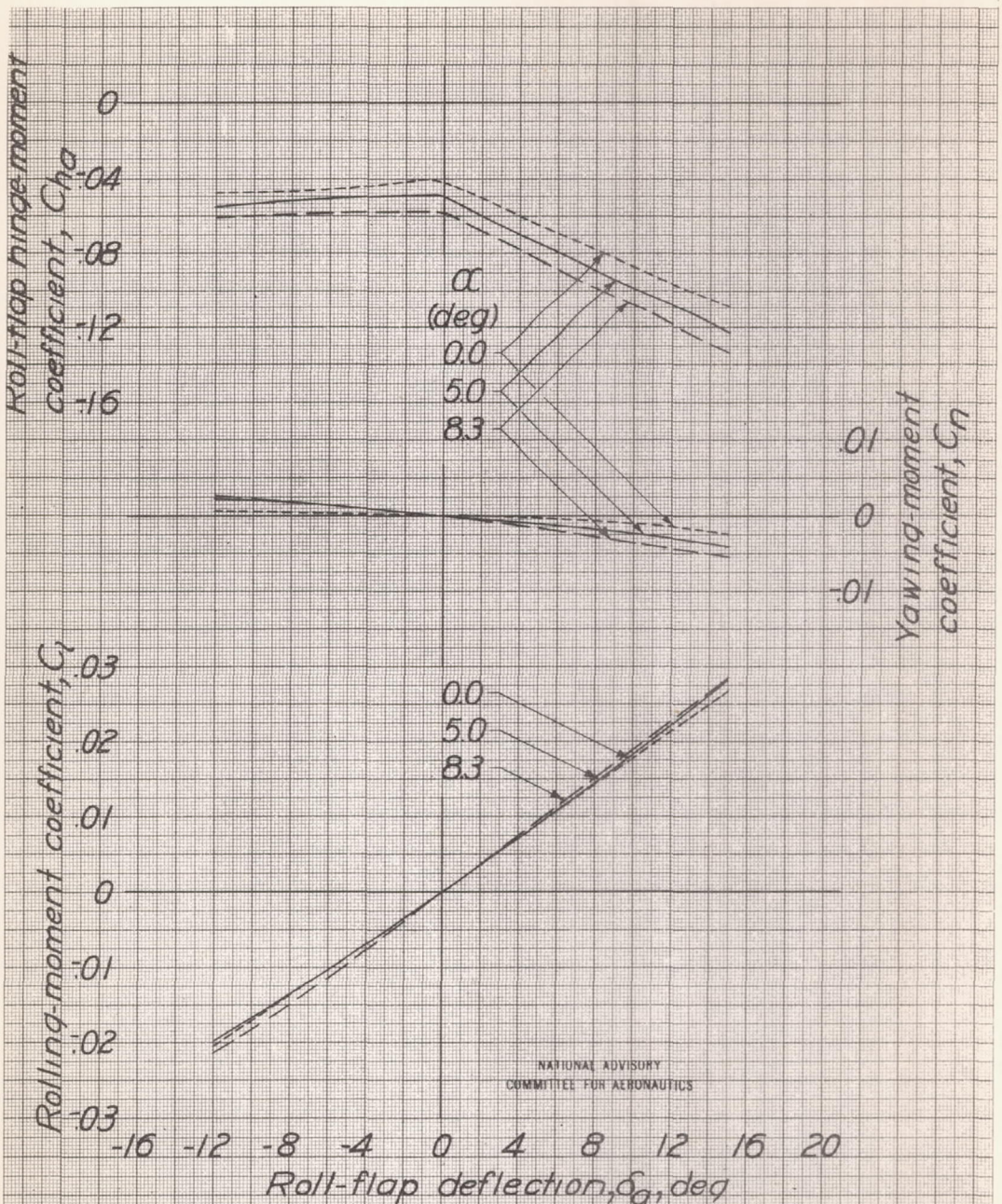

Figure 11.–Roll-flap characteristics with full-span flaps 30-percent extended. Standard model configuration $\delta_f = 0°$; $R \approx 5{,}200{,}000$; $M \approx 0.12$.

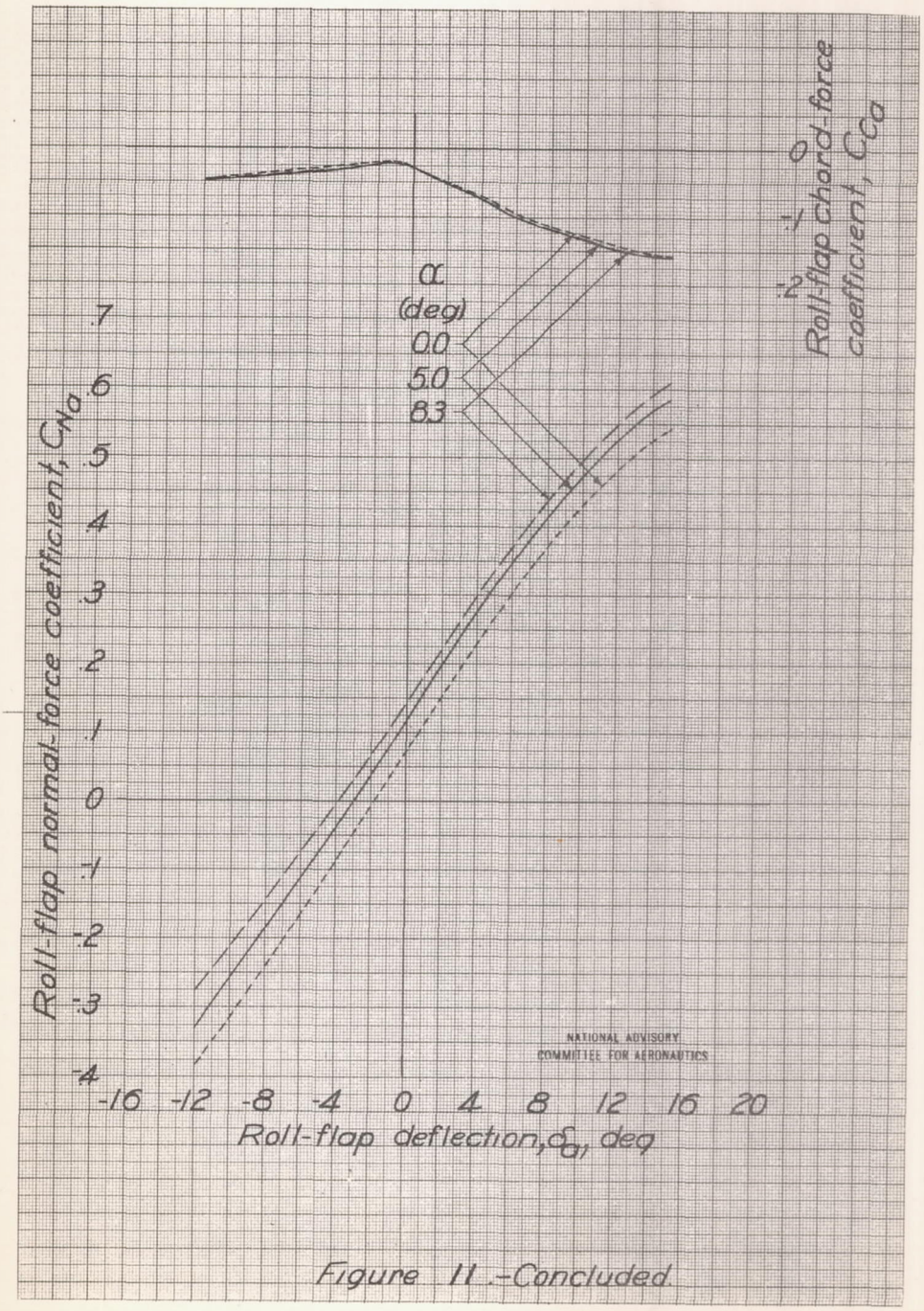

Figure 11.-Concluded.

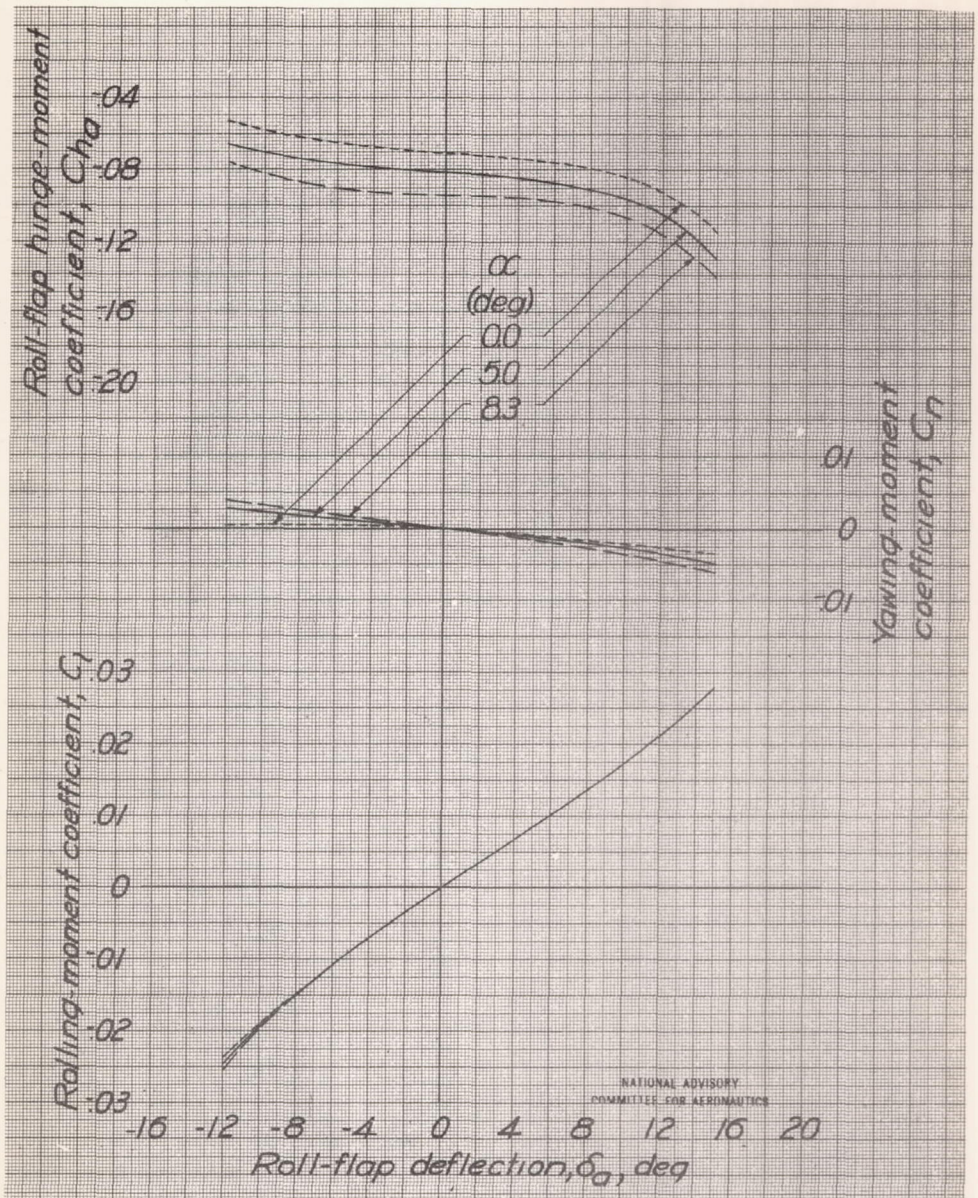

Figure 12.- Roll-flap characteristics with full-span flaps 50-percent extended. Standard model configuration; $\delta_f = 0°$; $R \approx 5{,}200{,}000$, $M \approx 0.12$.

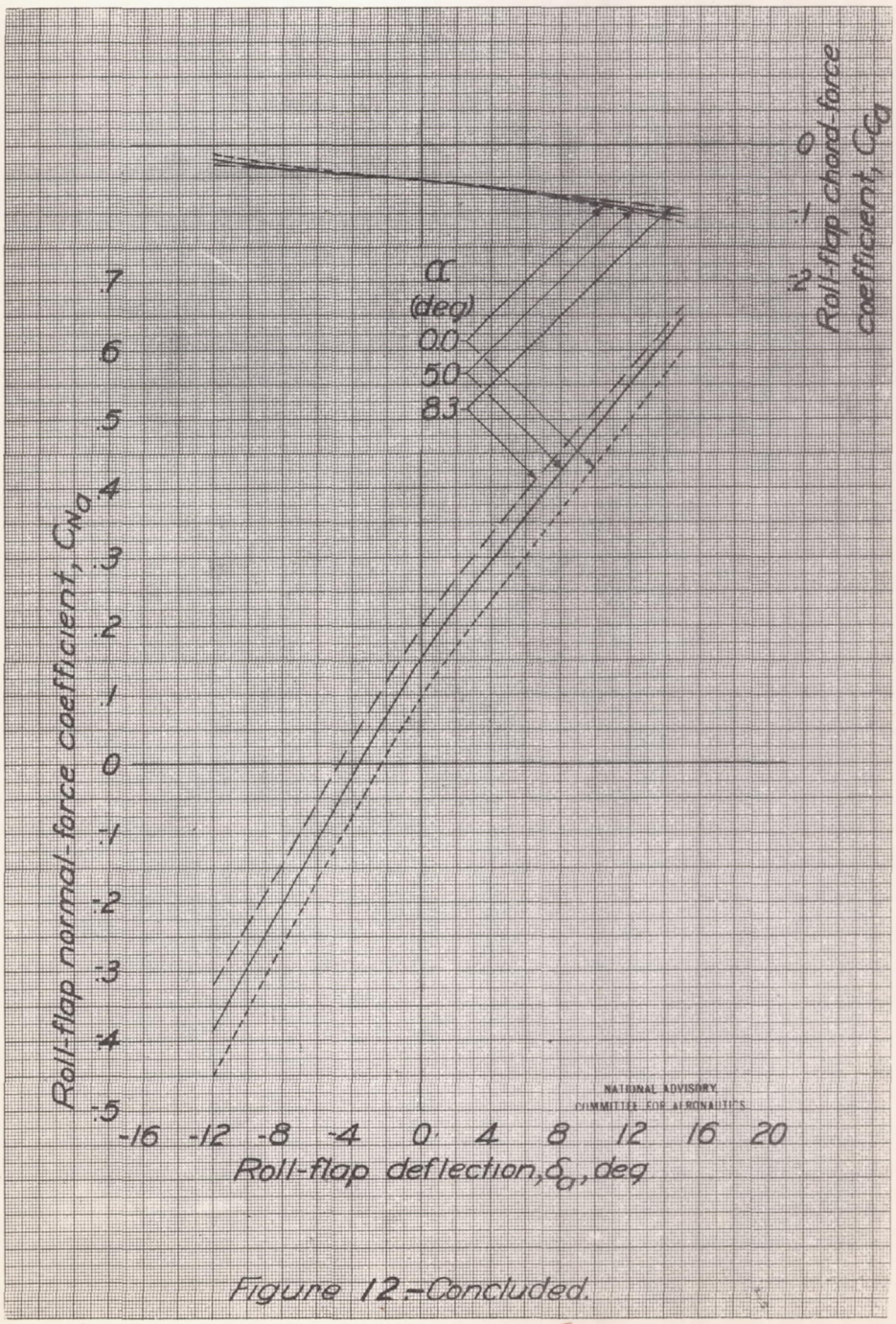

Figure 12.-Concluded.

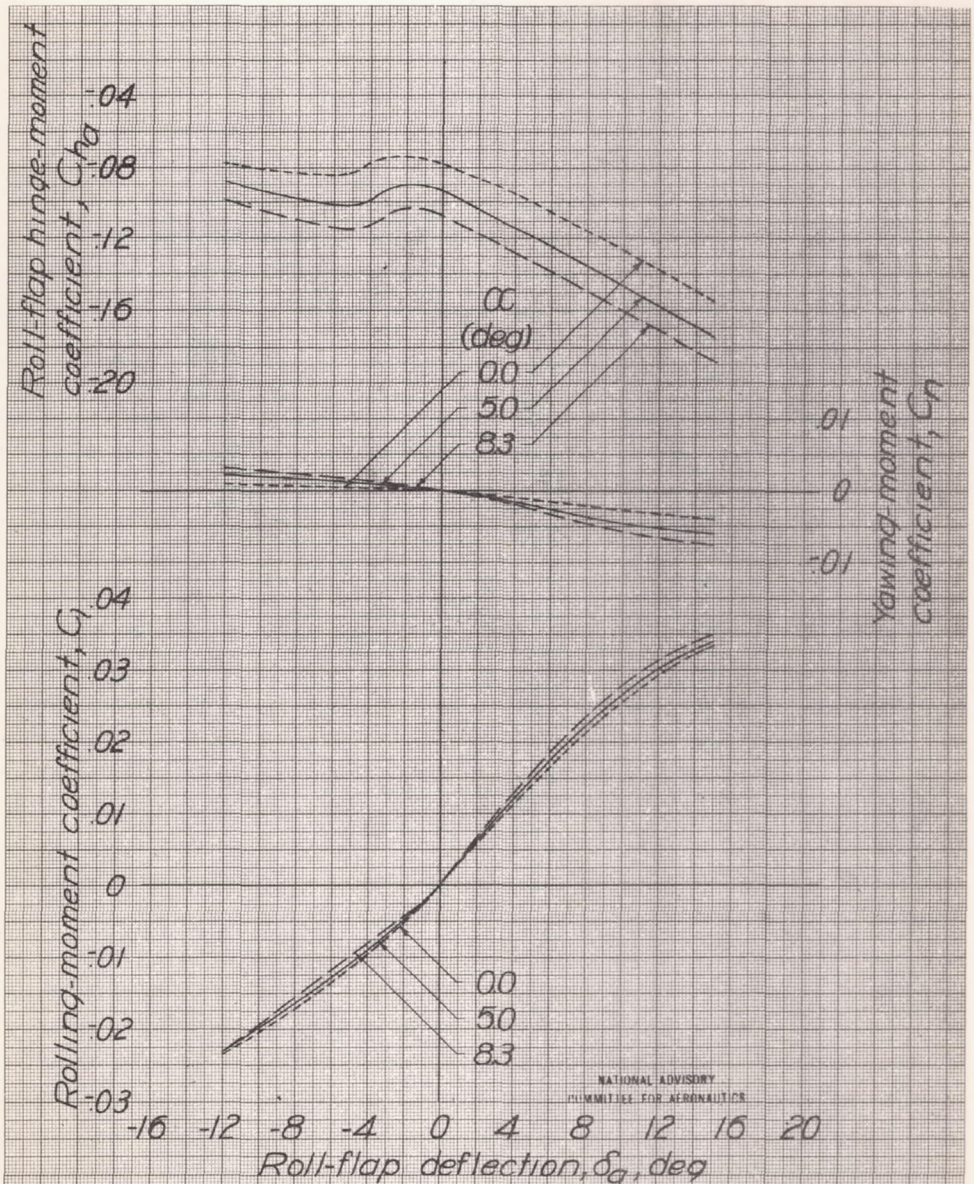

Figure 13.- Roll-flap characteristics with full-span flaps 70-percent extended. Standard model configuration; $\delta_f = 7°$; $R \approx 5,200,000$, $M \approx 0.12$.

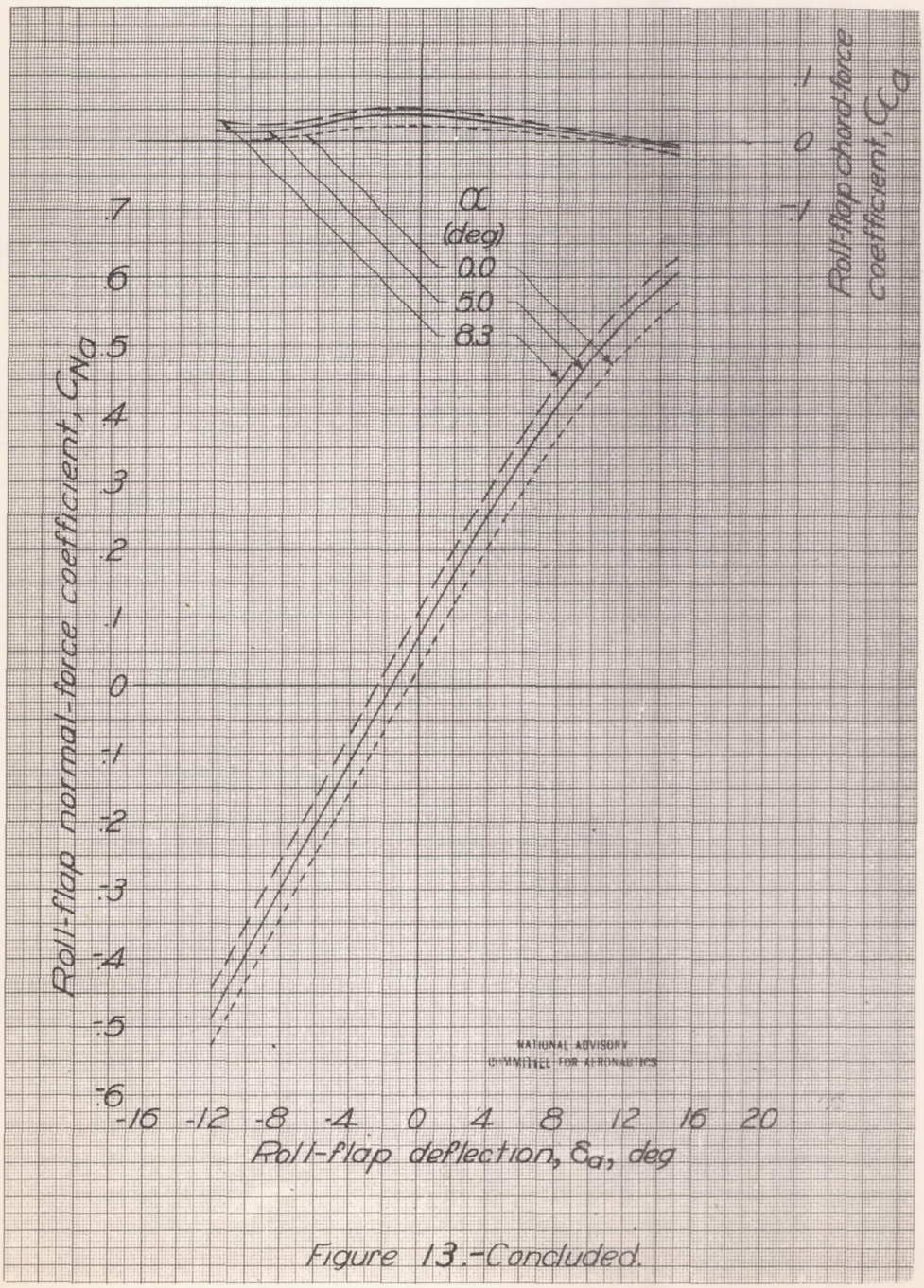

Figure 13.-Concluded.

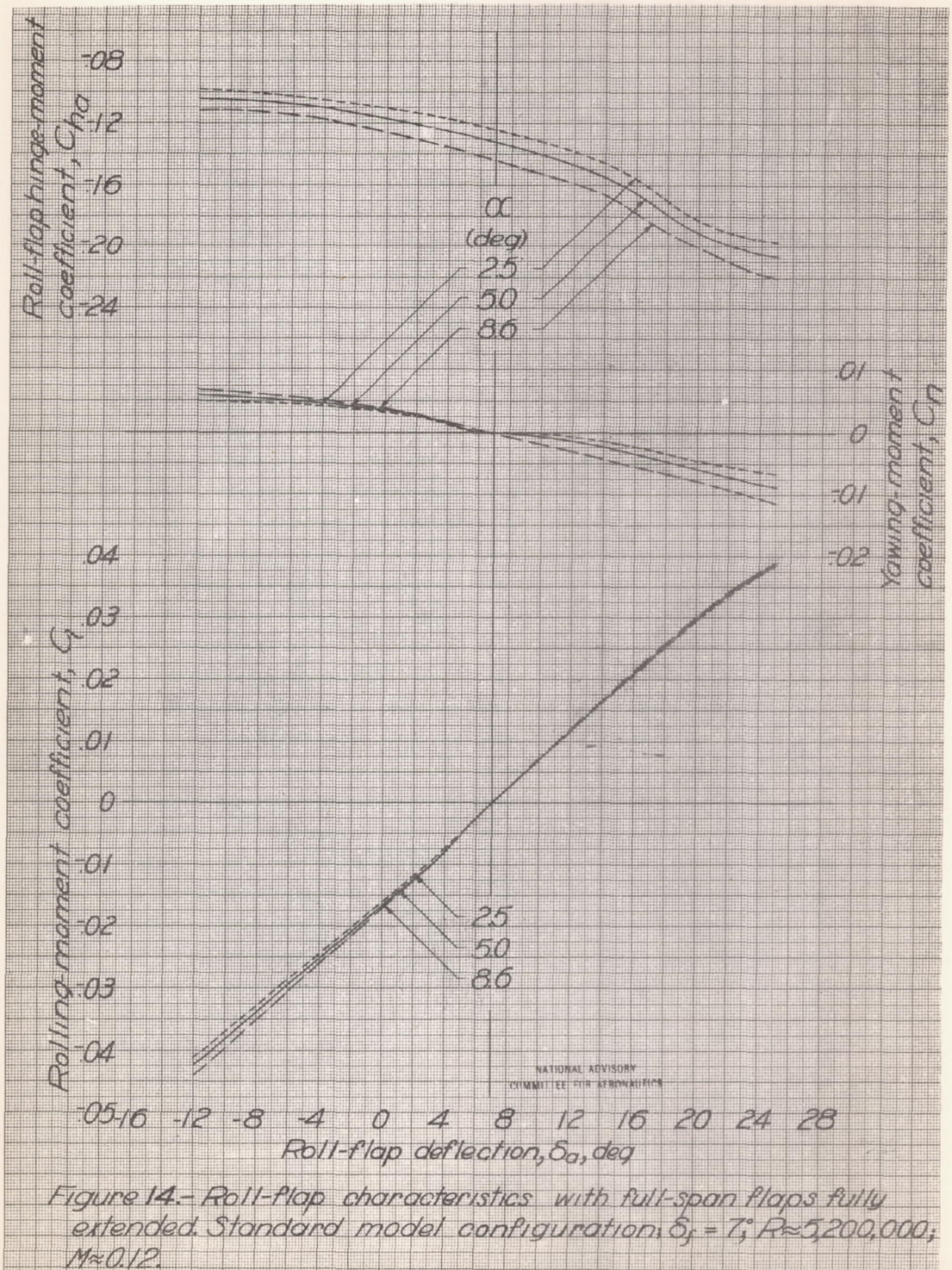

Figure 14.- Roll-flap characteristics with full-span flaps fully extended. Standard model configuration: $\delta_f = 7°$; $R \approx 5{,}200{,}000$; $M \approx 0.12$.

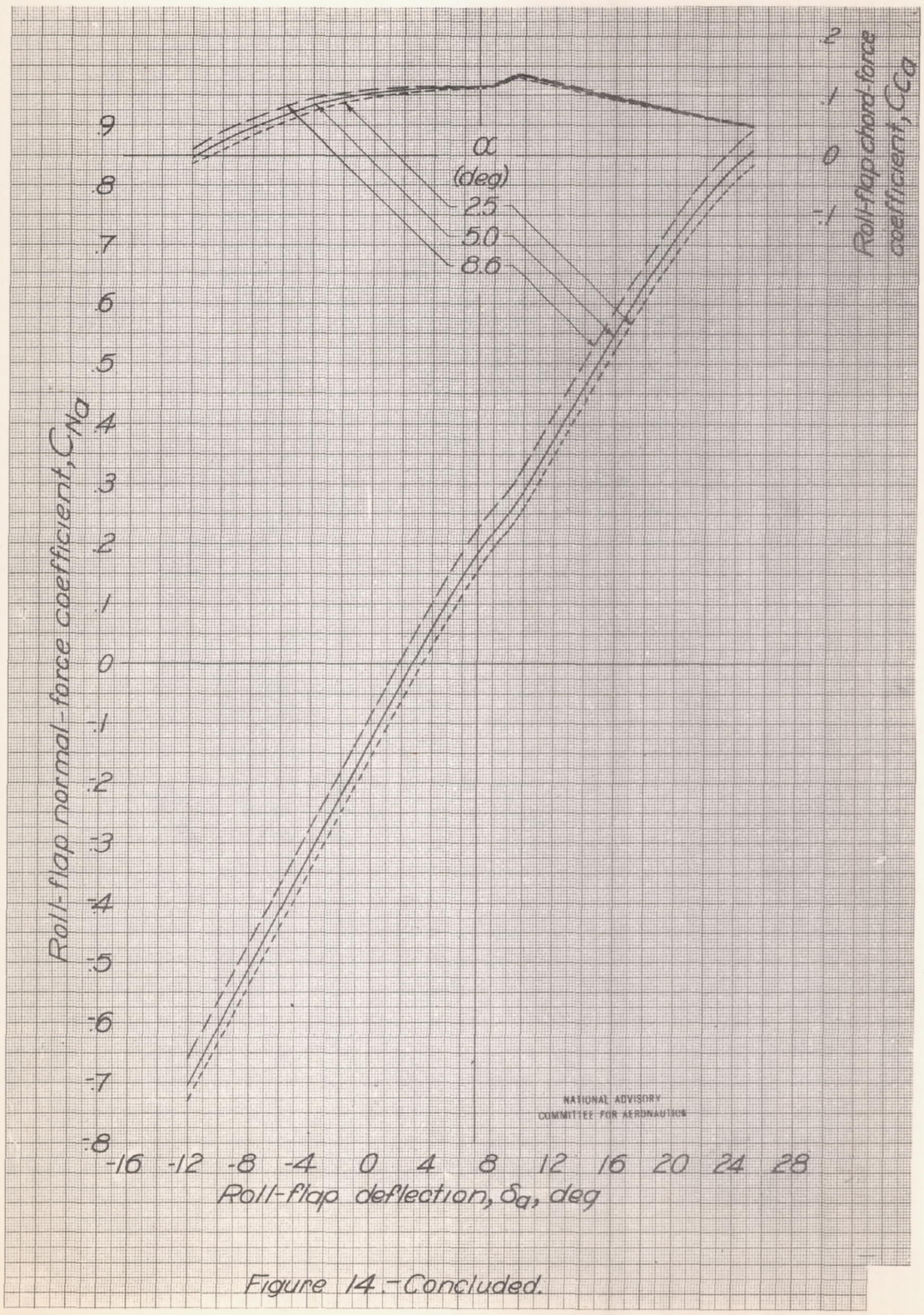

Figure 14.- Concluded.

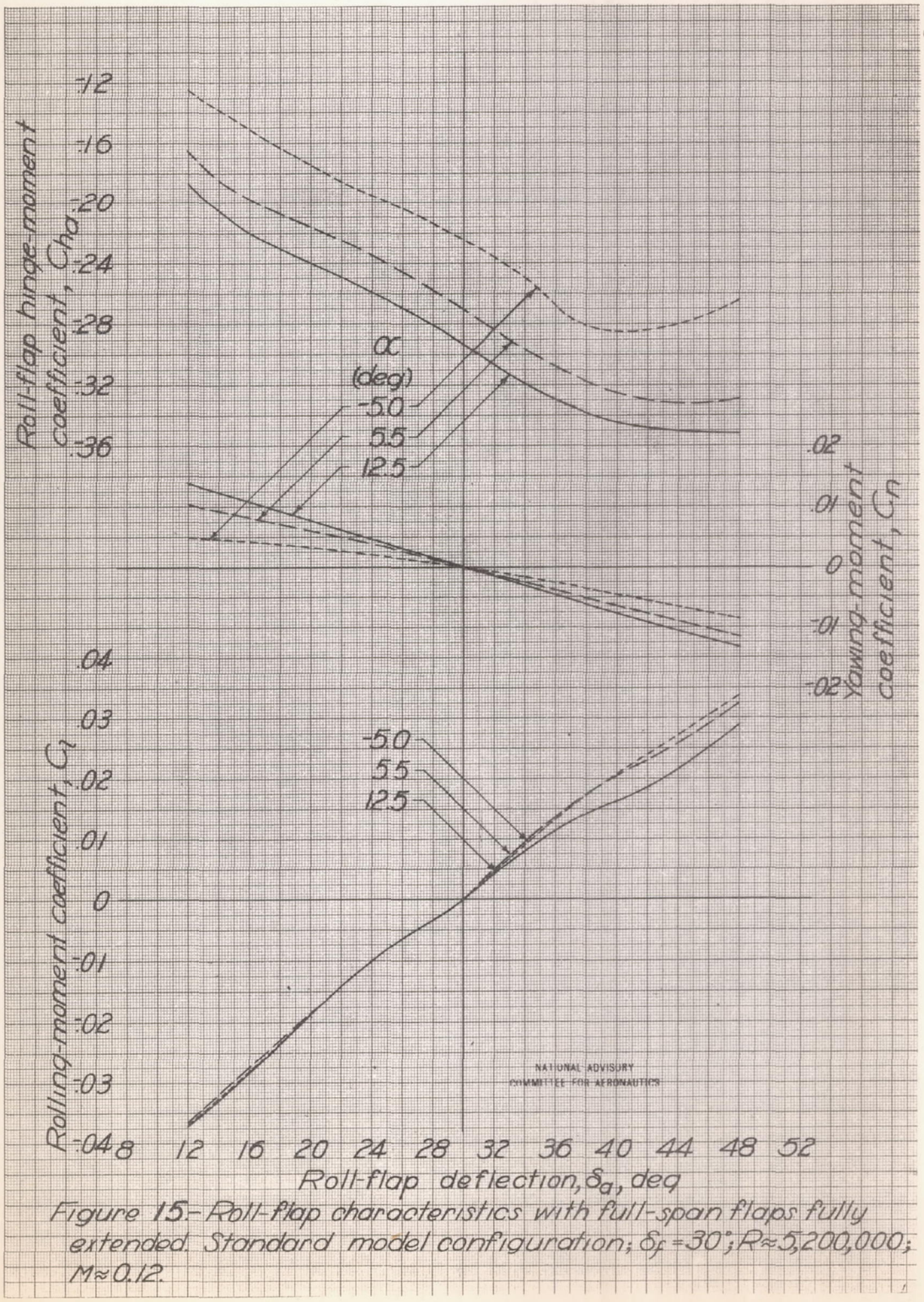

Figure 15.- Roll-flap characteristics with full-span flaps fully extended. Standard model configuration; $\delta_f = 30°$; $R \approx 5{,}200{,}000$; $M \approx 0.12$.

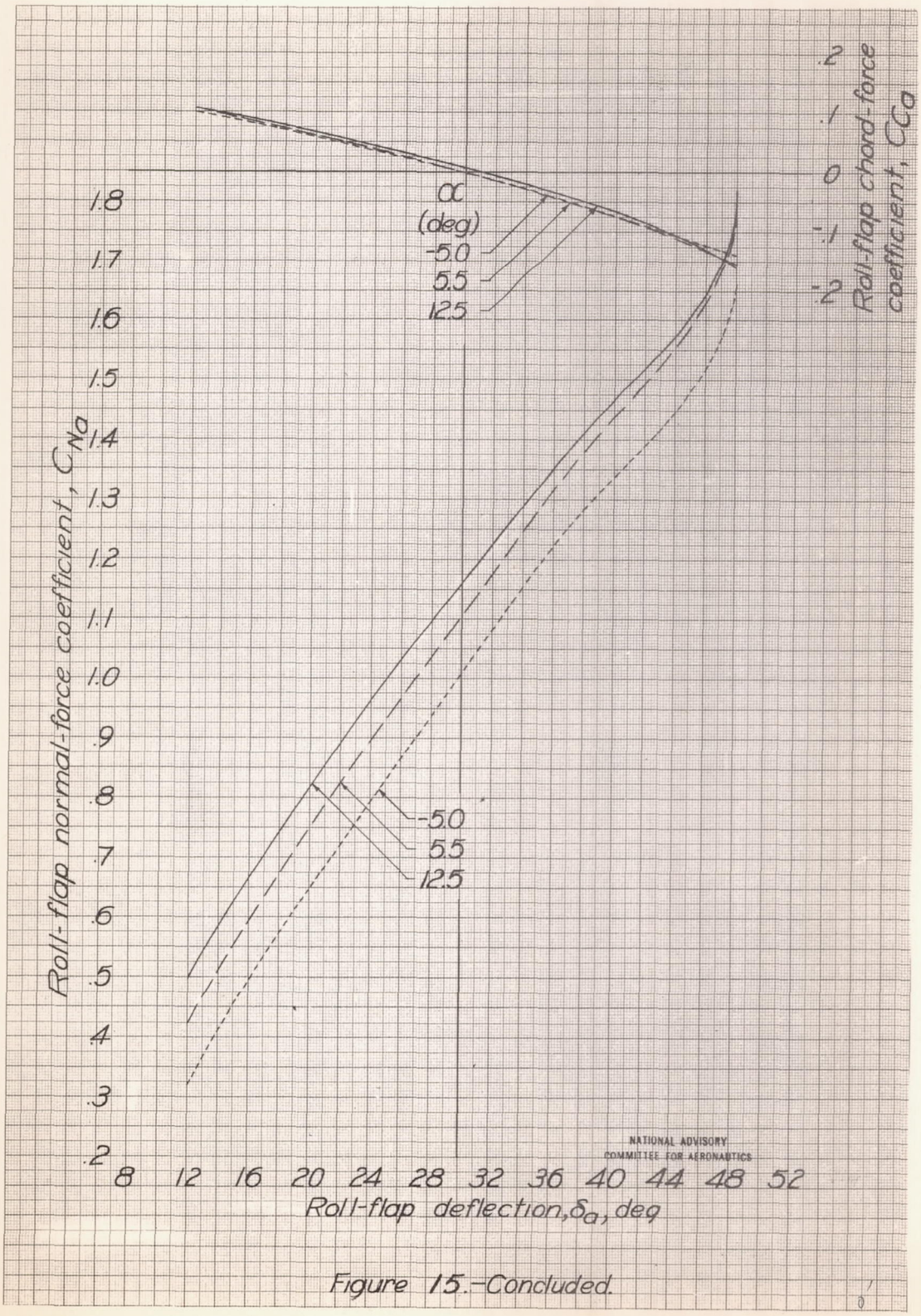

Figure 15.–Concluded.

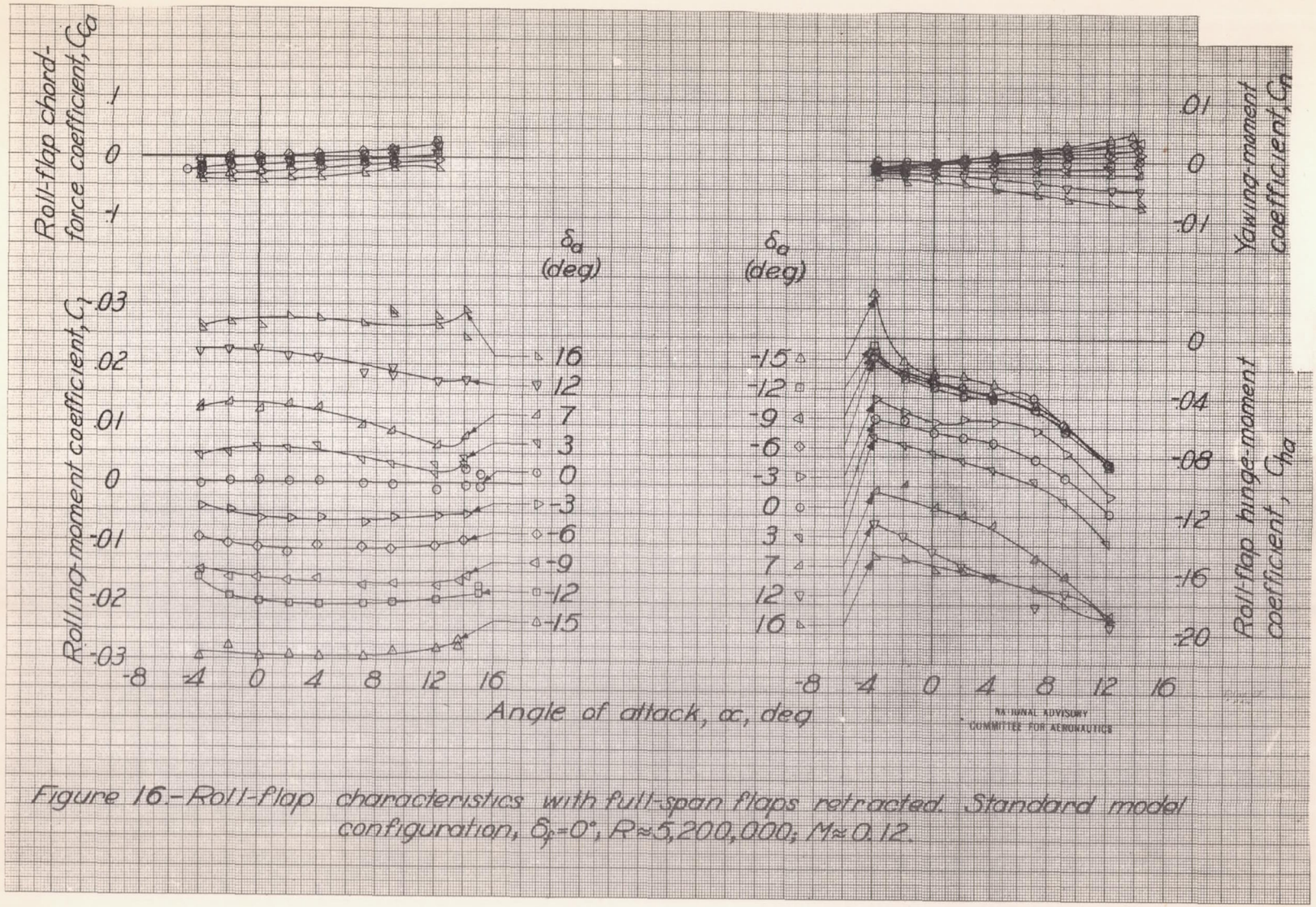

Figure 16.- Roll-flap characteristics with full-span flaps retracted. Standard model configuration, δ_f=0°; R≈5,200,000; M≈0.12.

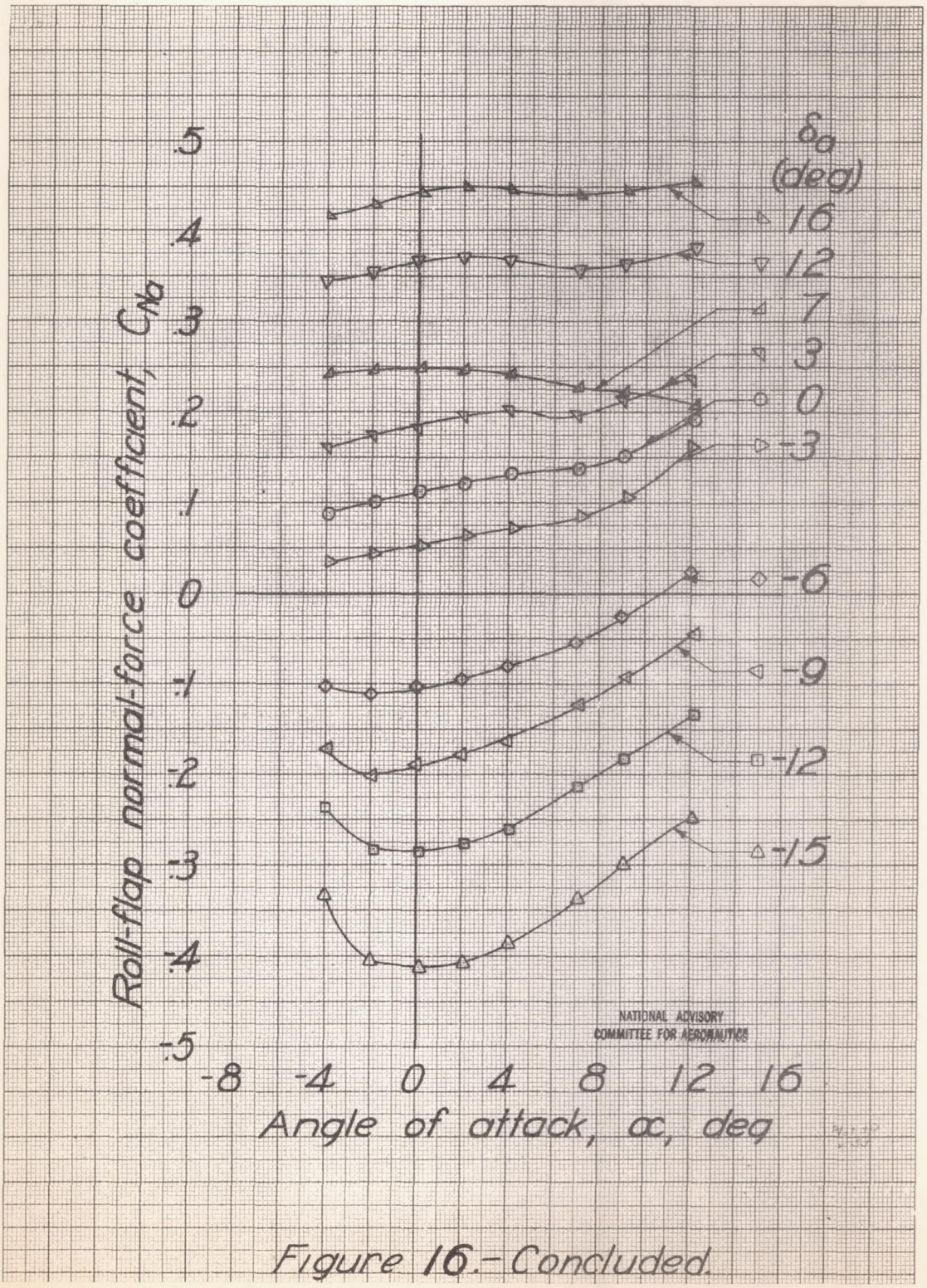

Figure 16.- Concluded.

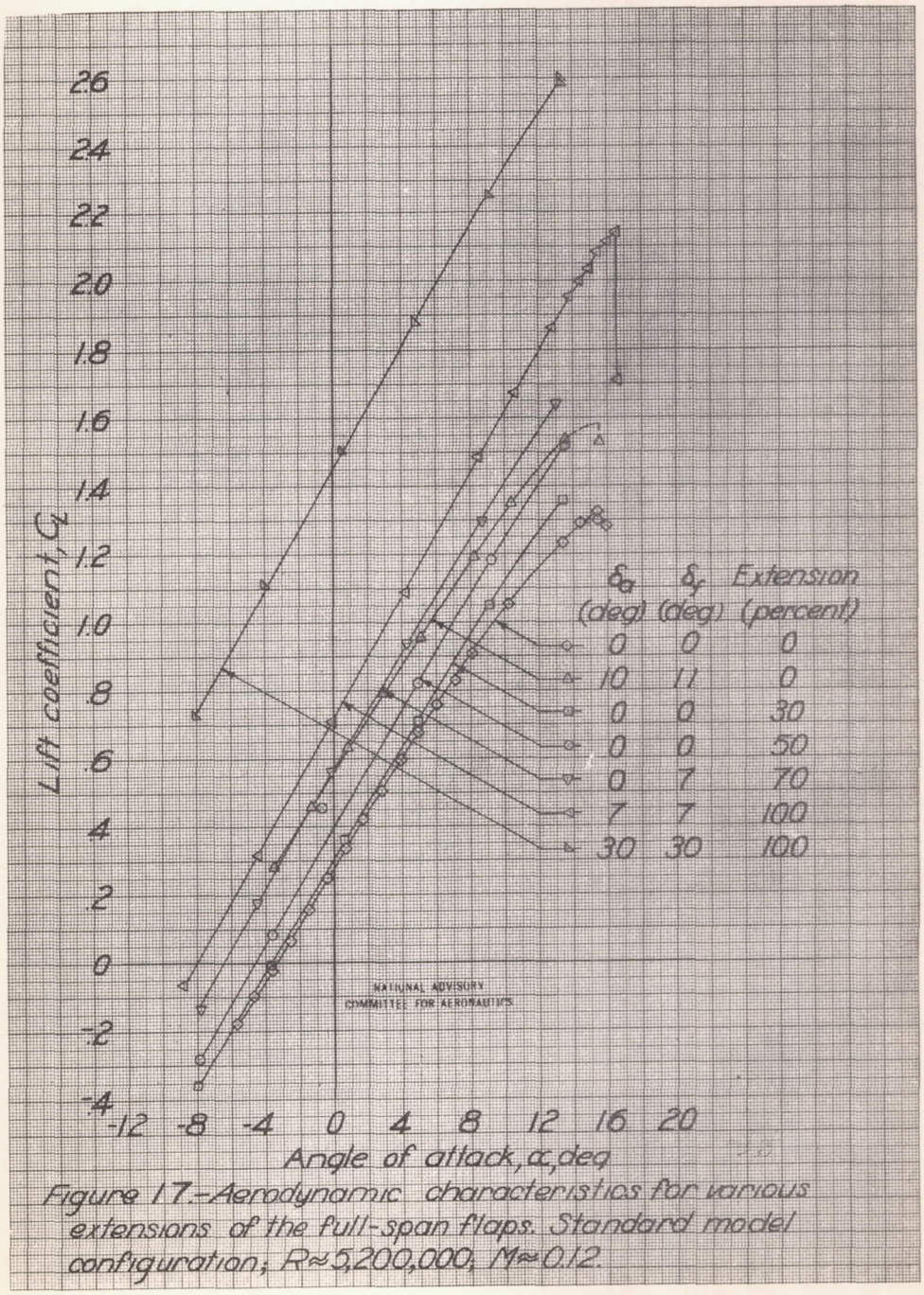

Figure 17.-Aerodynamic characteristics for various extensions of the full-span flaps. Standard model configuration; $R \approx 5,200,000$, $M \approx 0.12$.

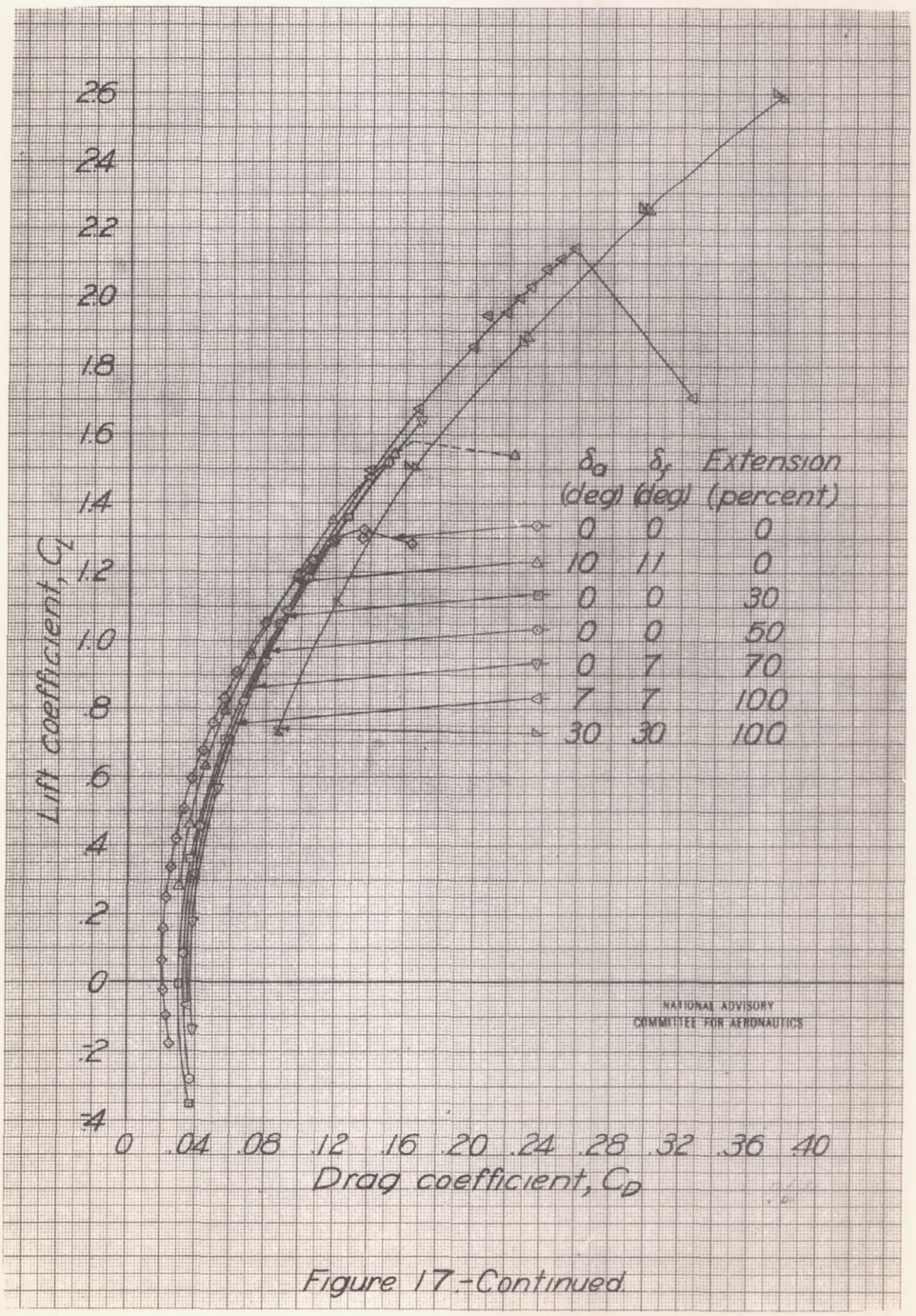

Figure 17.-Continued

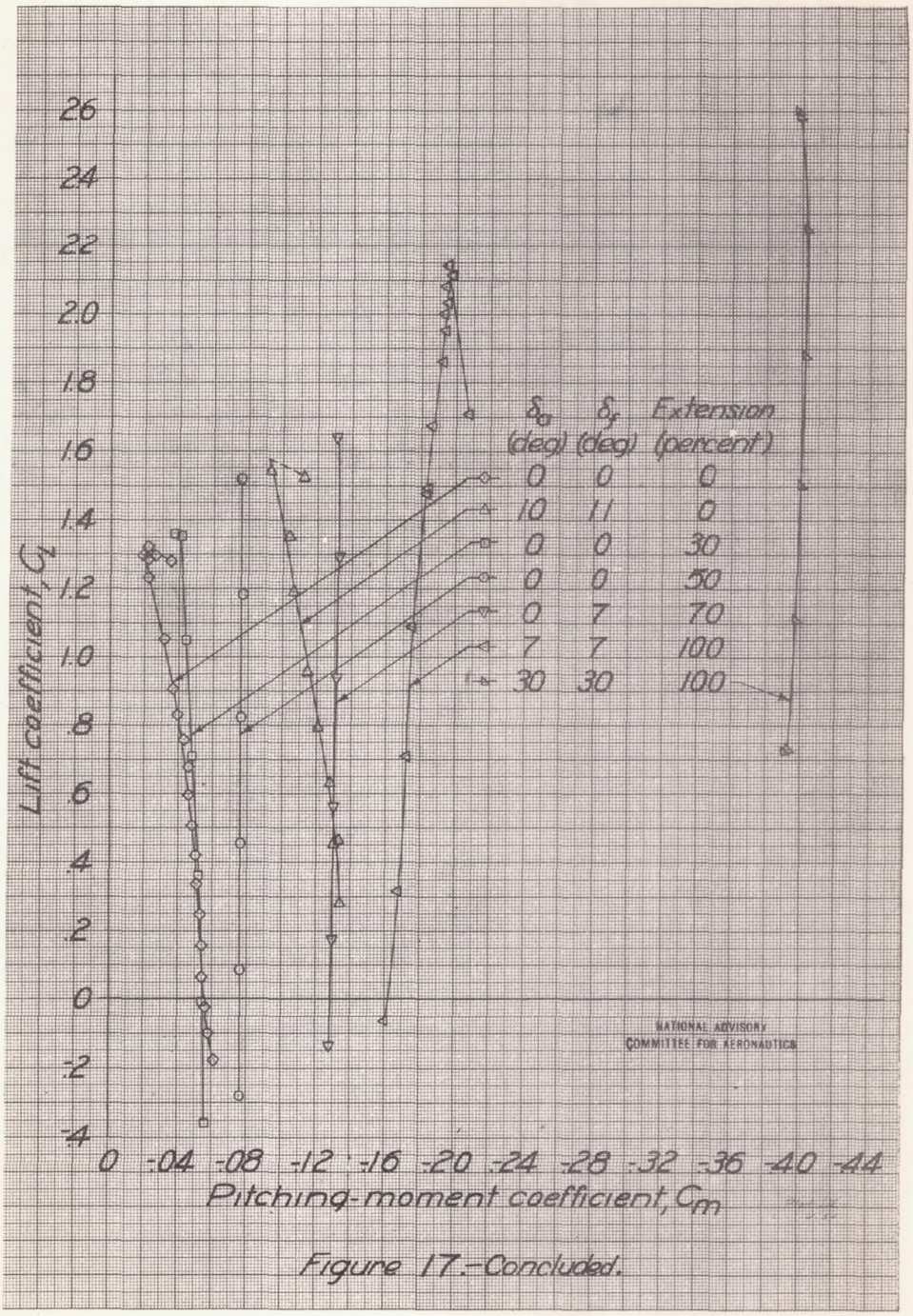

Figure 17.-Concluded.

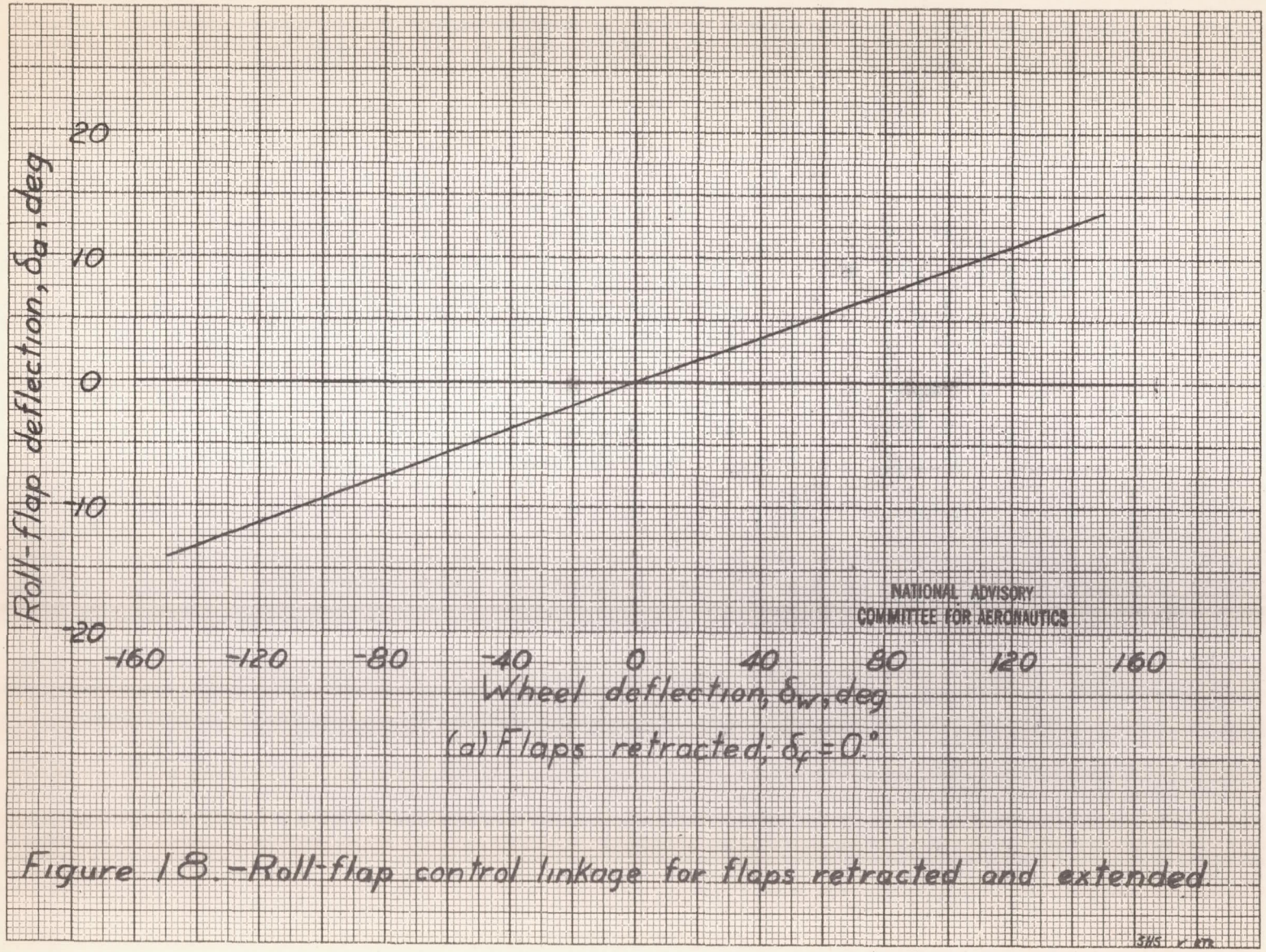

(a) Flaps retracted; $\delta_f = 0°$

Figure 18.—Roll-flap control linkage for flaps retracted and extended.

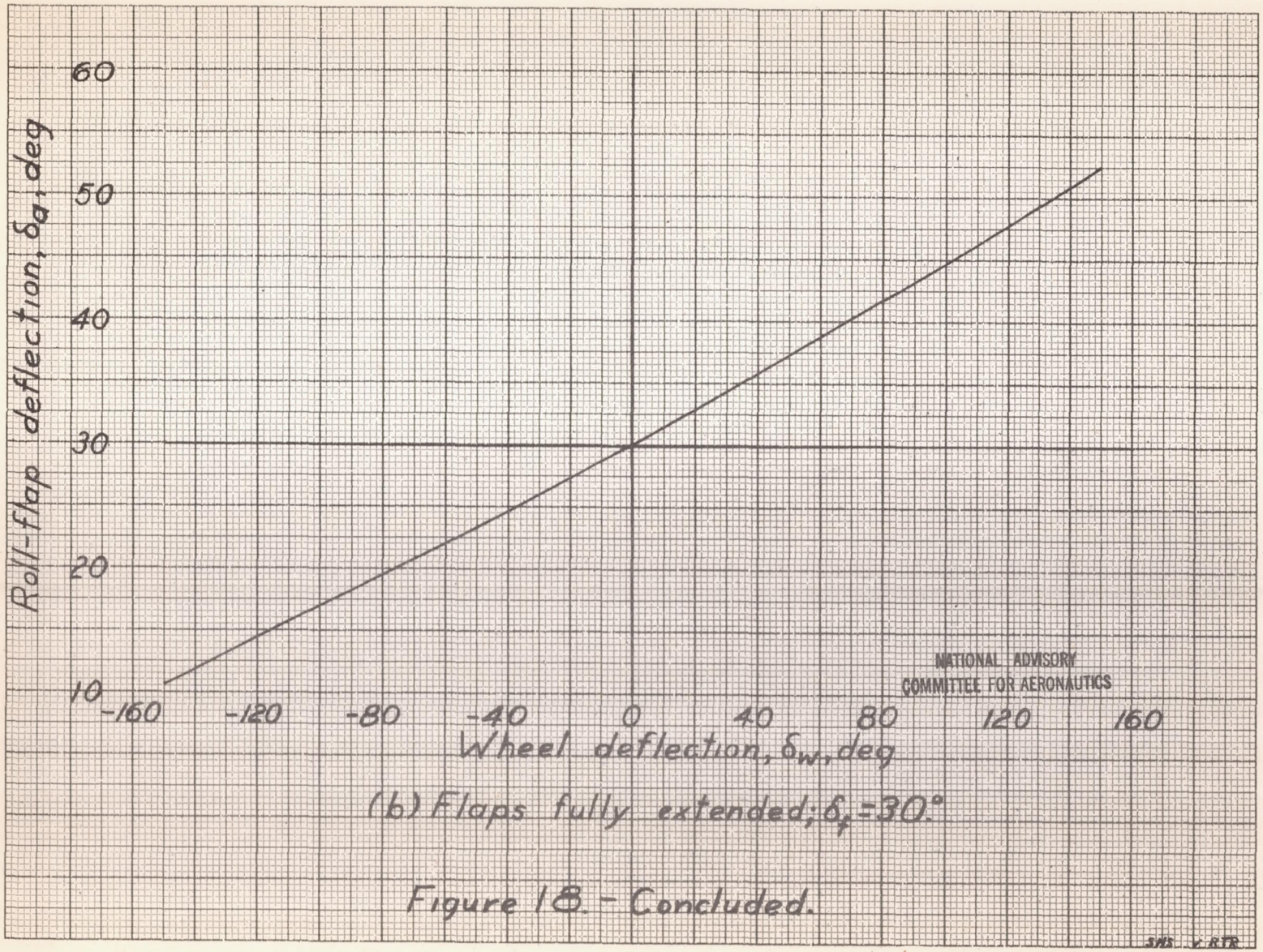

(b) Flaps fully extended; $\delta_f = 30°$

Figure 18. - Concluded.

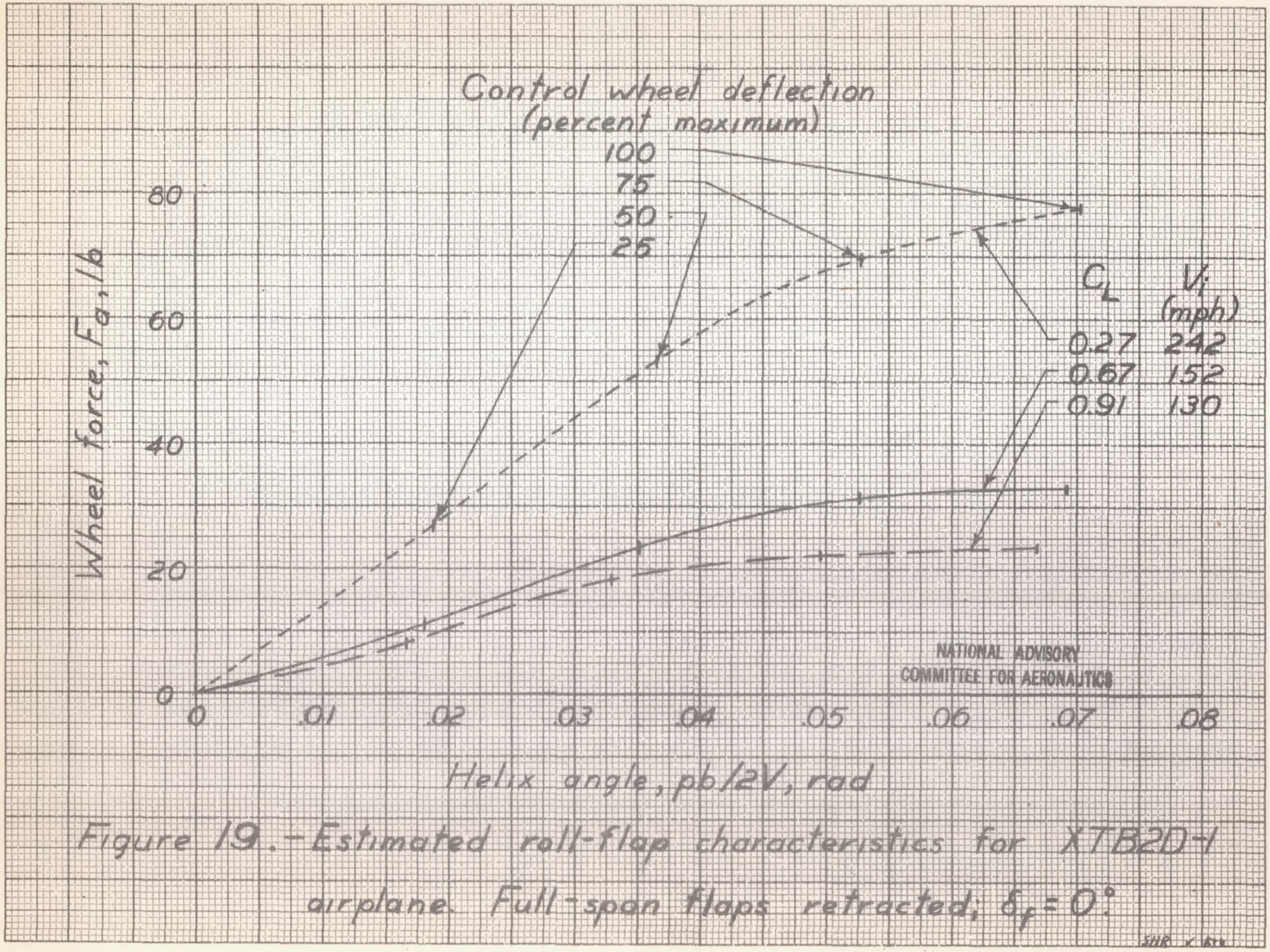

Figure 19.- Estimated roll-flap characteristics for XTB2D-1 airplane. Full-span flaps retracted; $\delta_f = 0°$.

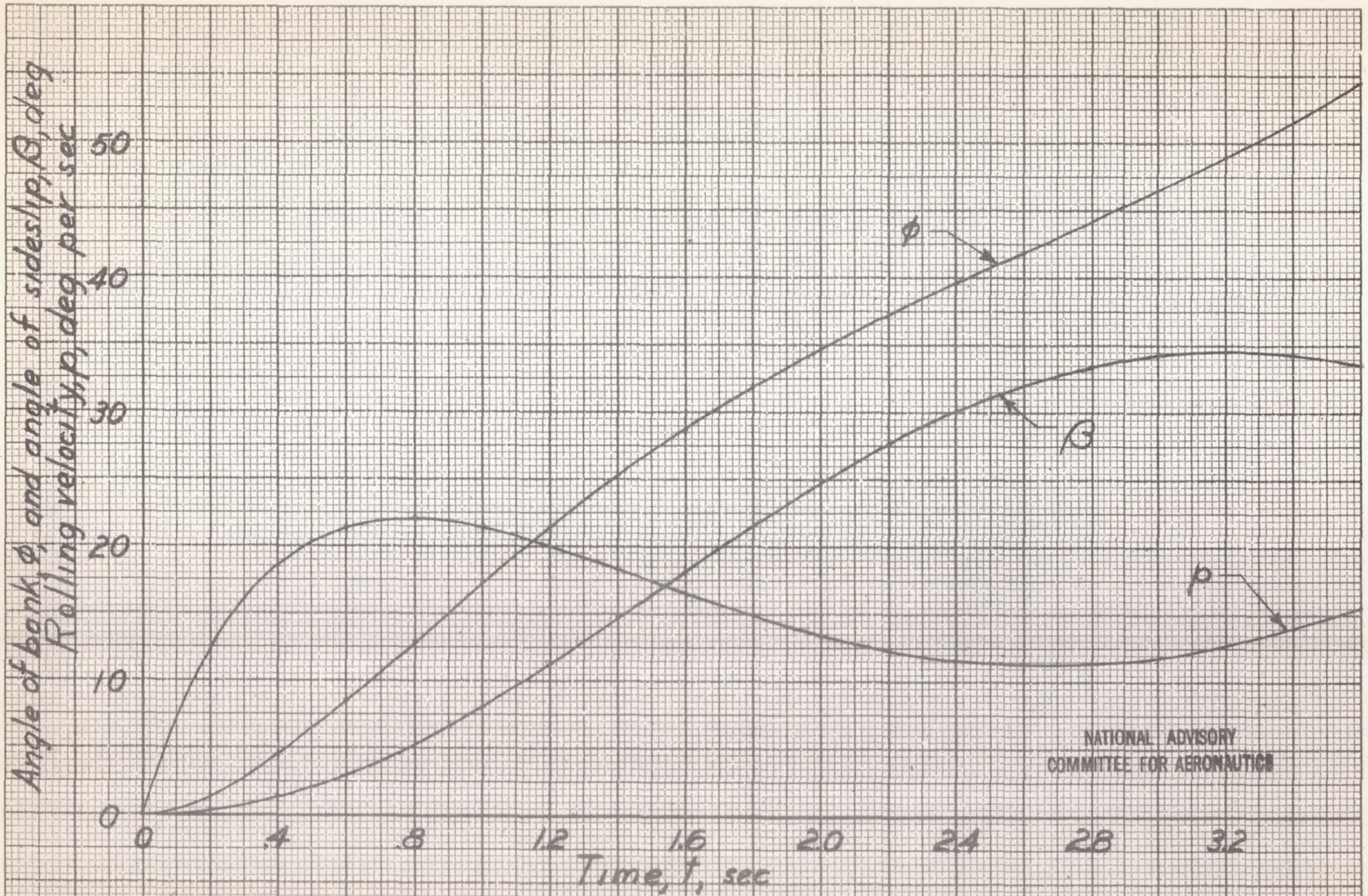

Figure 20.- Time history of the XTB2D-1 airplane following abrupt full roll-flap deflection. Full-span flaps deflected 30°; V_i = 92 mph.

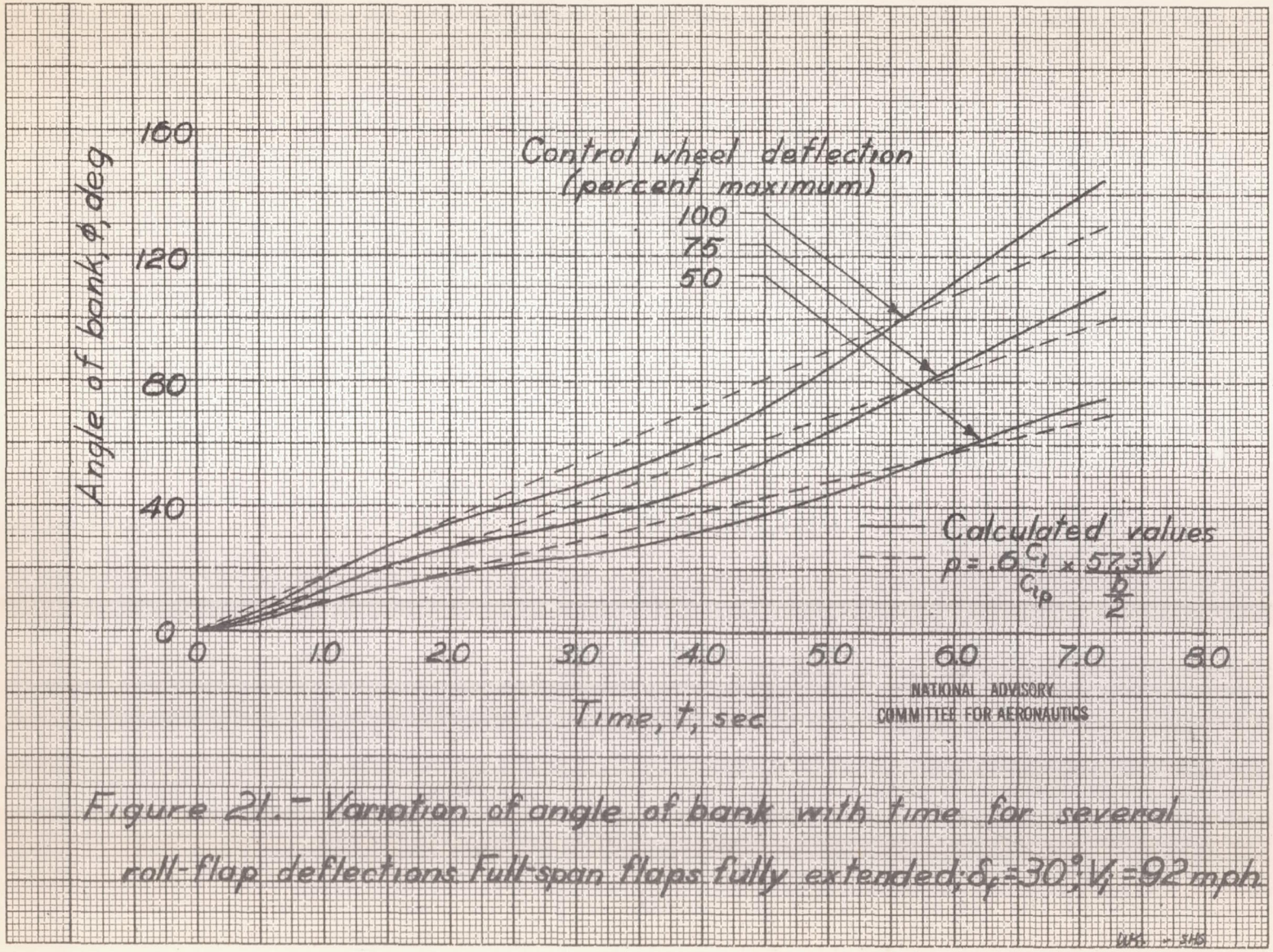

Figure 21. - Variation of angle of bank with time for several roll-flap deflections. Full-span flaps fully extended; $\delta_f = 30°$; $V_i = 92$ mph.

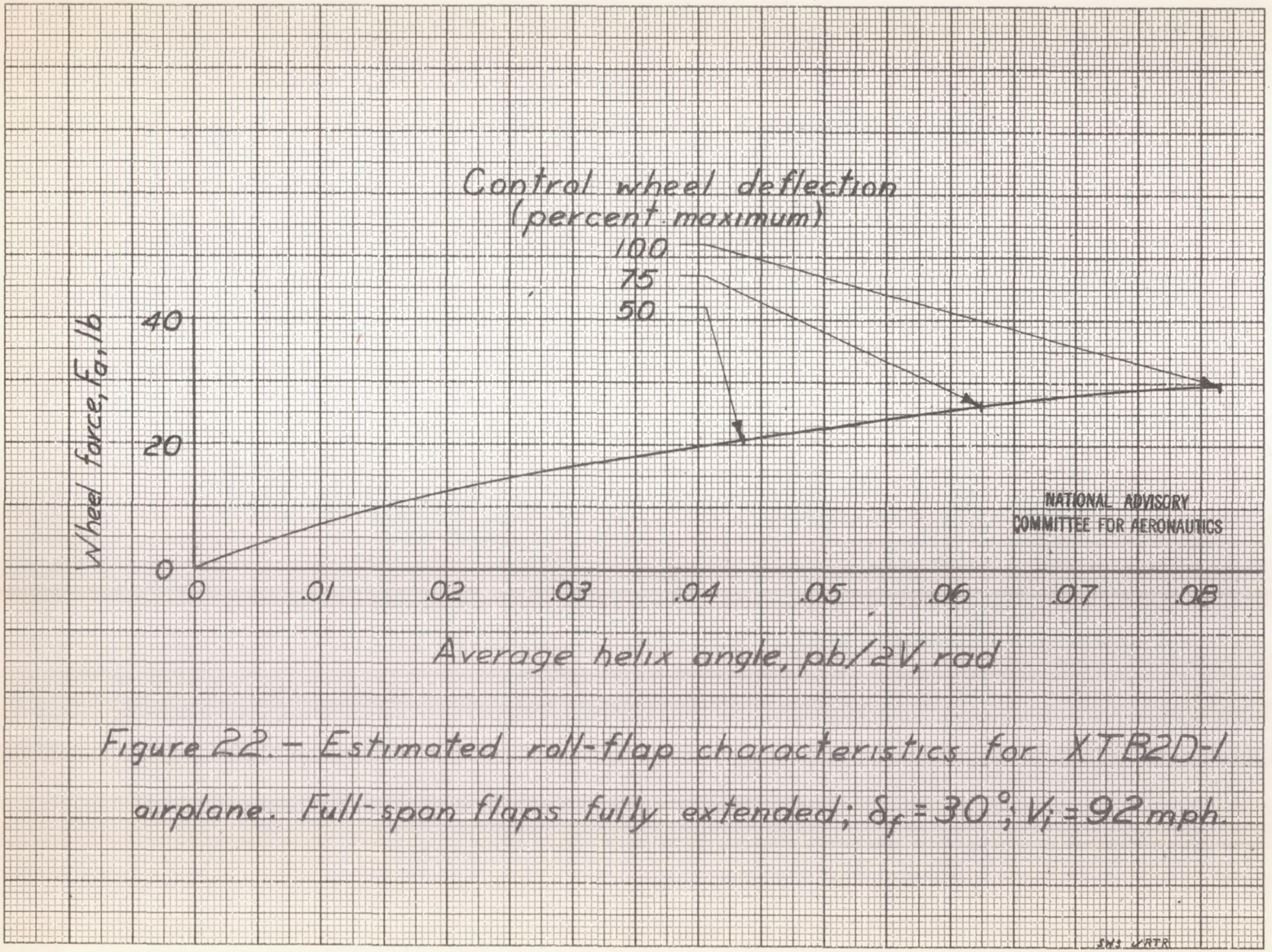

Figure 22.- Estimated roll-flap characteristics for XTB2D-1 airplane. Full-span flaps fully extended; $\delta_f = 30°$; $V_i = 92$ mph.

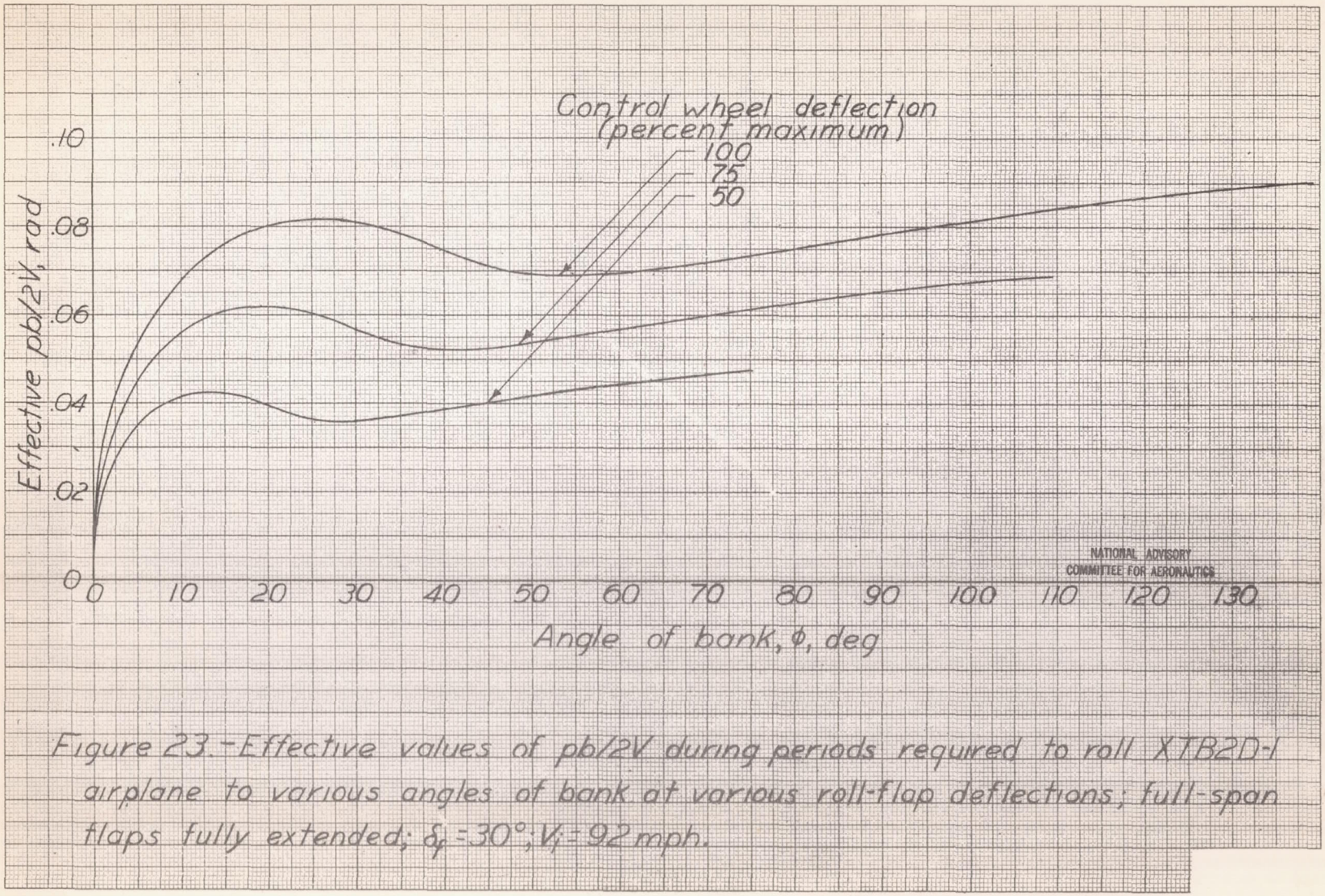

Figure 23.- Effective values of pb/2V during periods required to roll XTB2D-1 airplane to various angles of bank at various roll-flap deflections; full-span flaps fully extended; $\delta_f = 30°$; $V_i = 92$ mph.

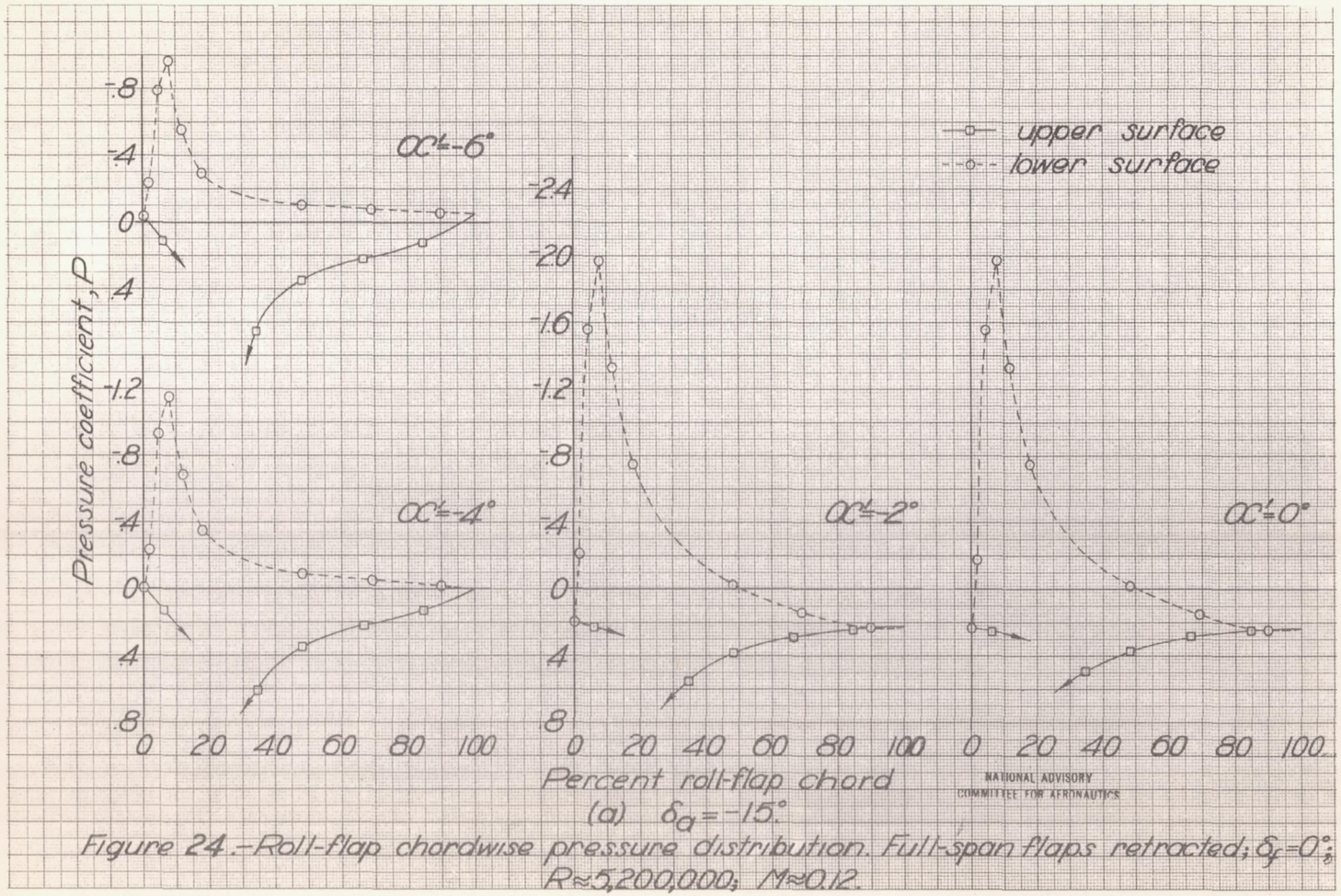

Figure 24.-Roll-flap chordwise pressure distribution. Full-span flaps retracted; $\delta_f = 0°$; $R \approx 5{,}200{,}000$; $M \approx 0.12$.

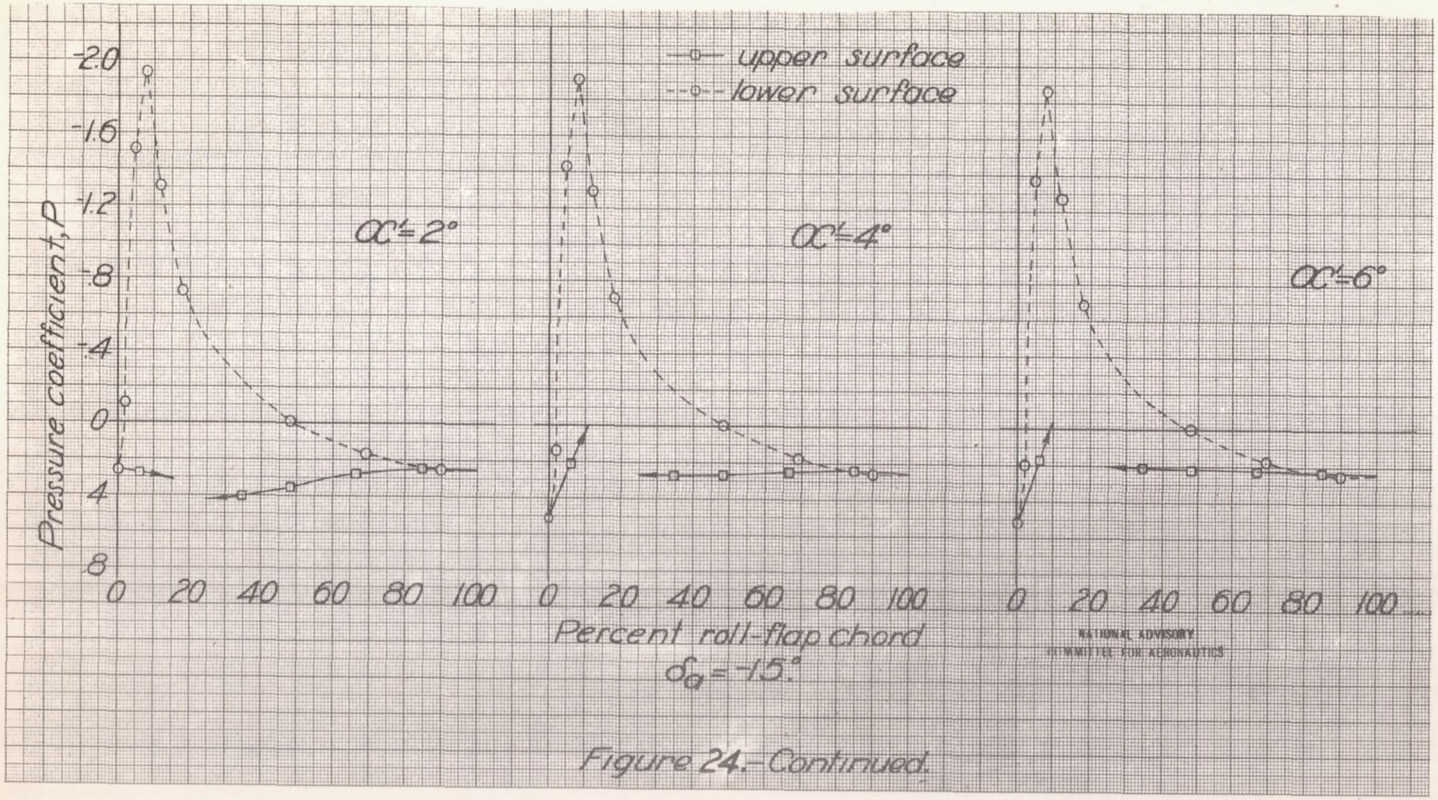

Figure 24.-Continued.

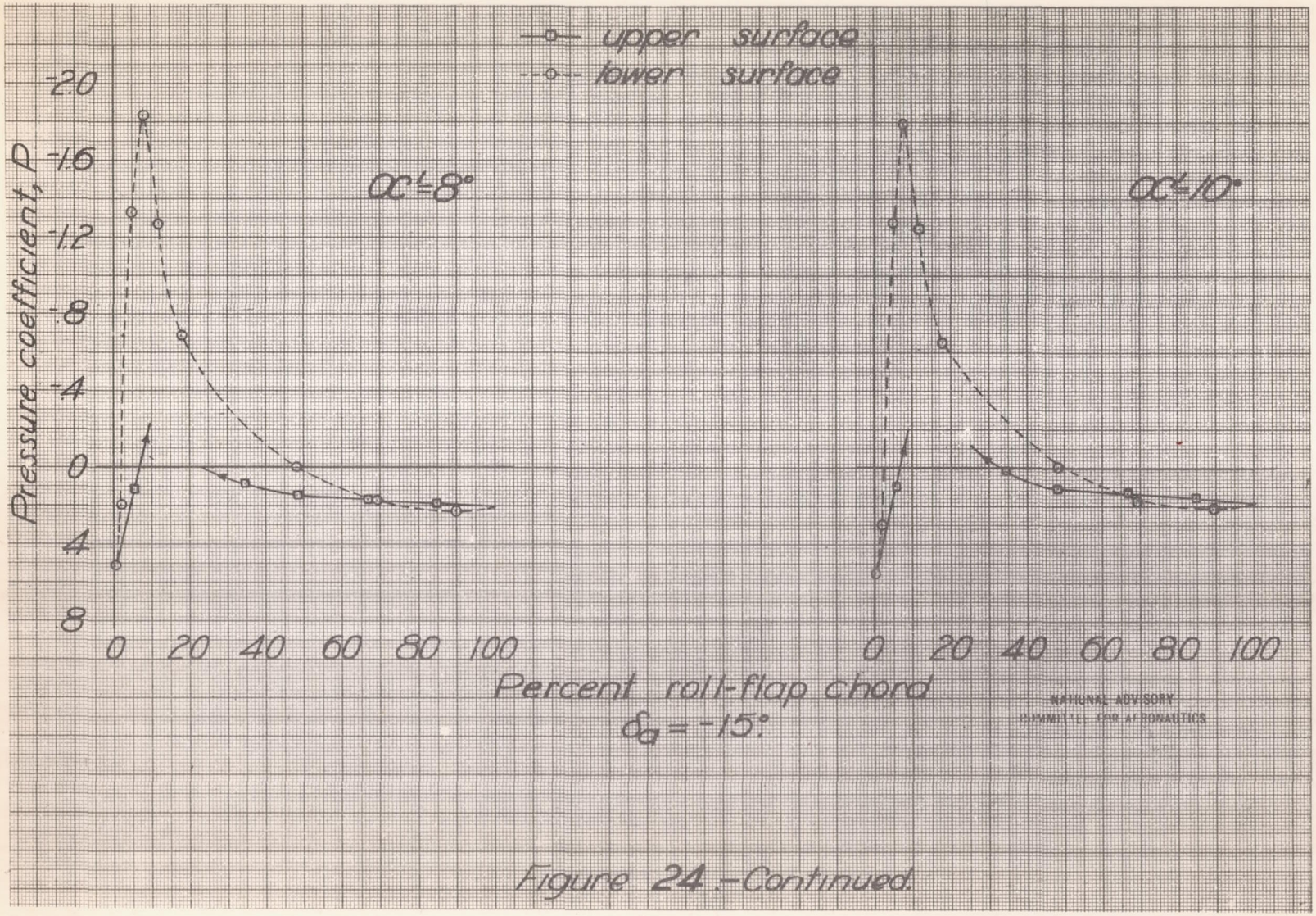

Figure 24.-Continued.

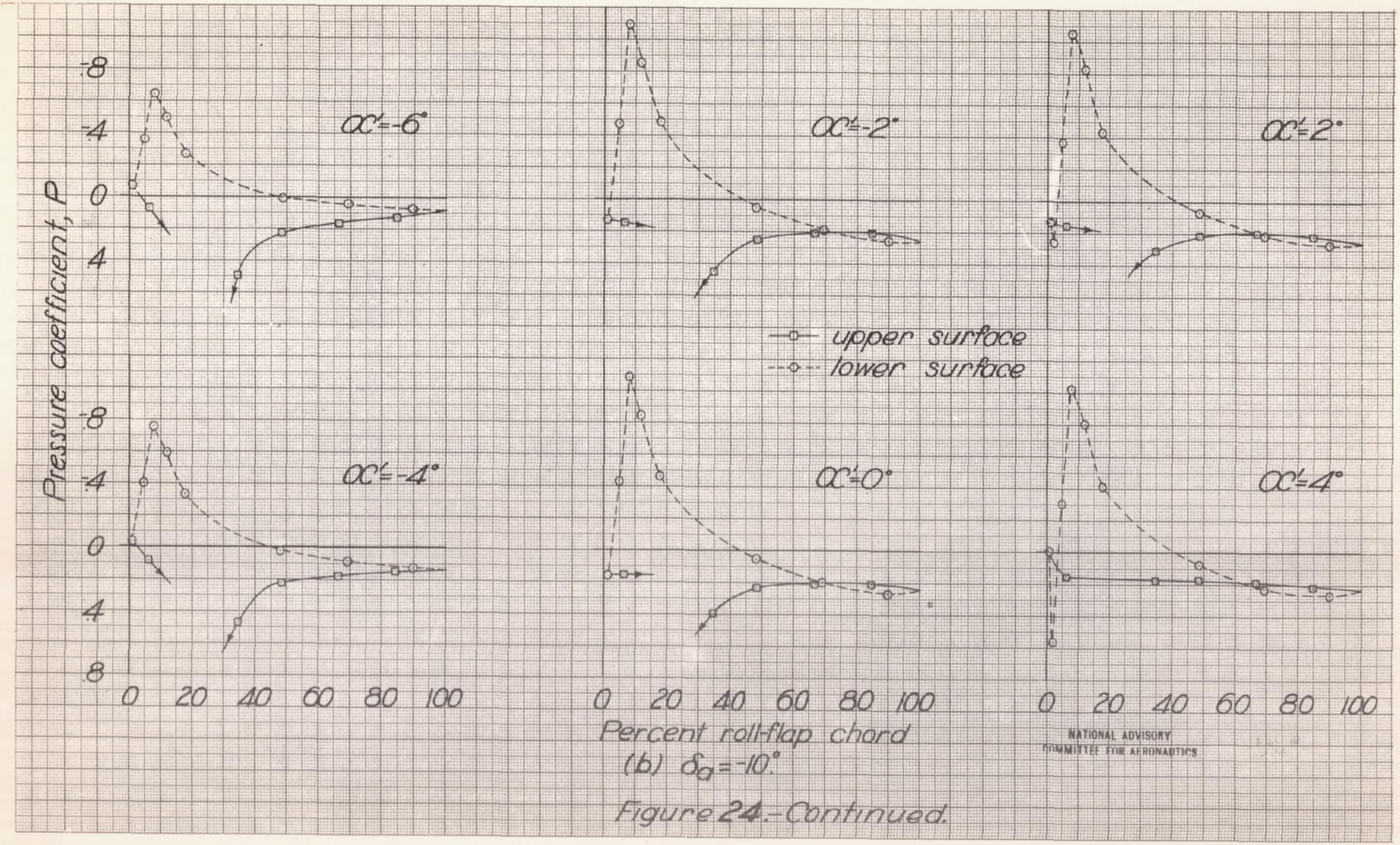

(b) $\delta_g = -10°$.

Figure 24.- Continued.

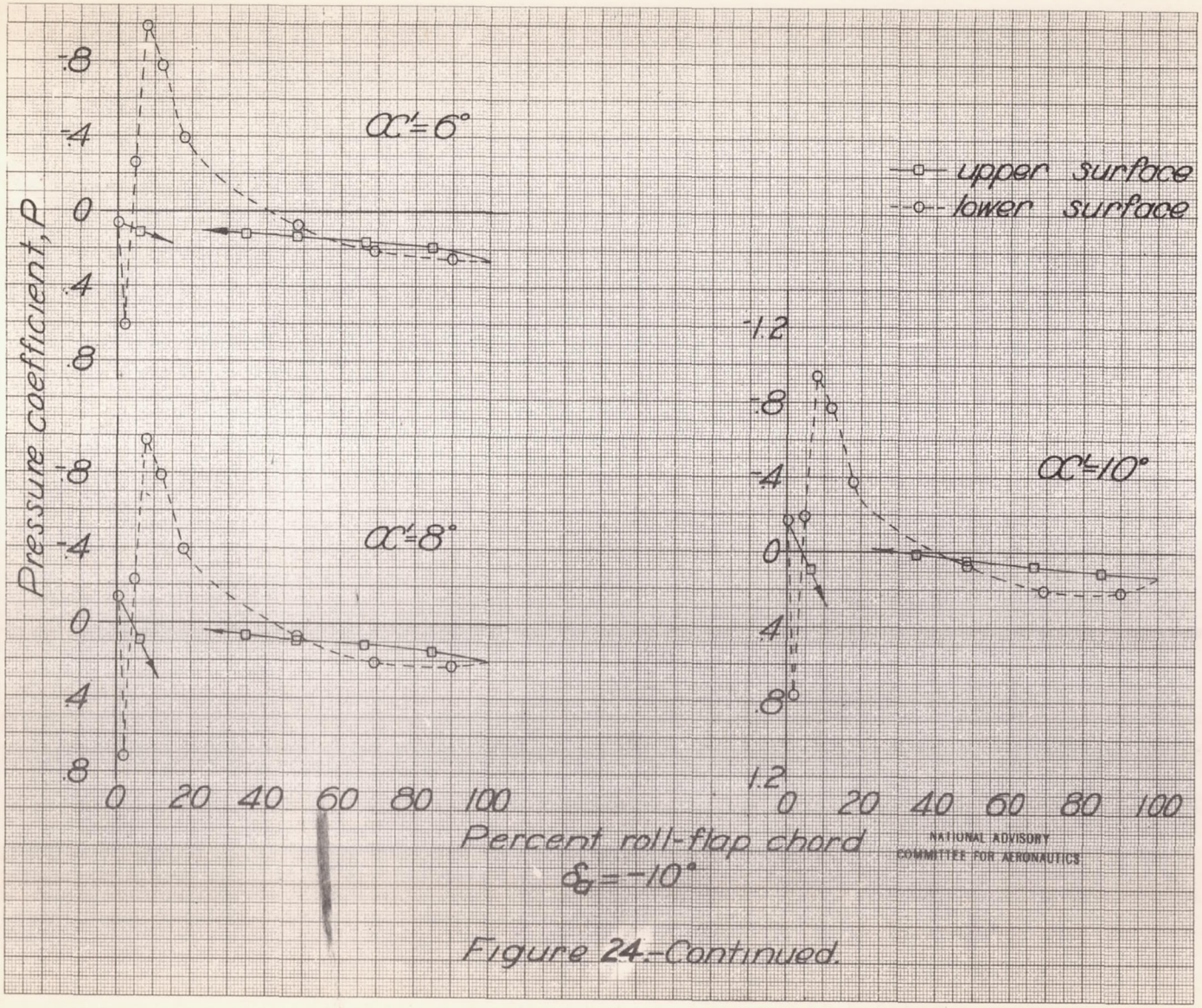

Figure 24.-Continued.

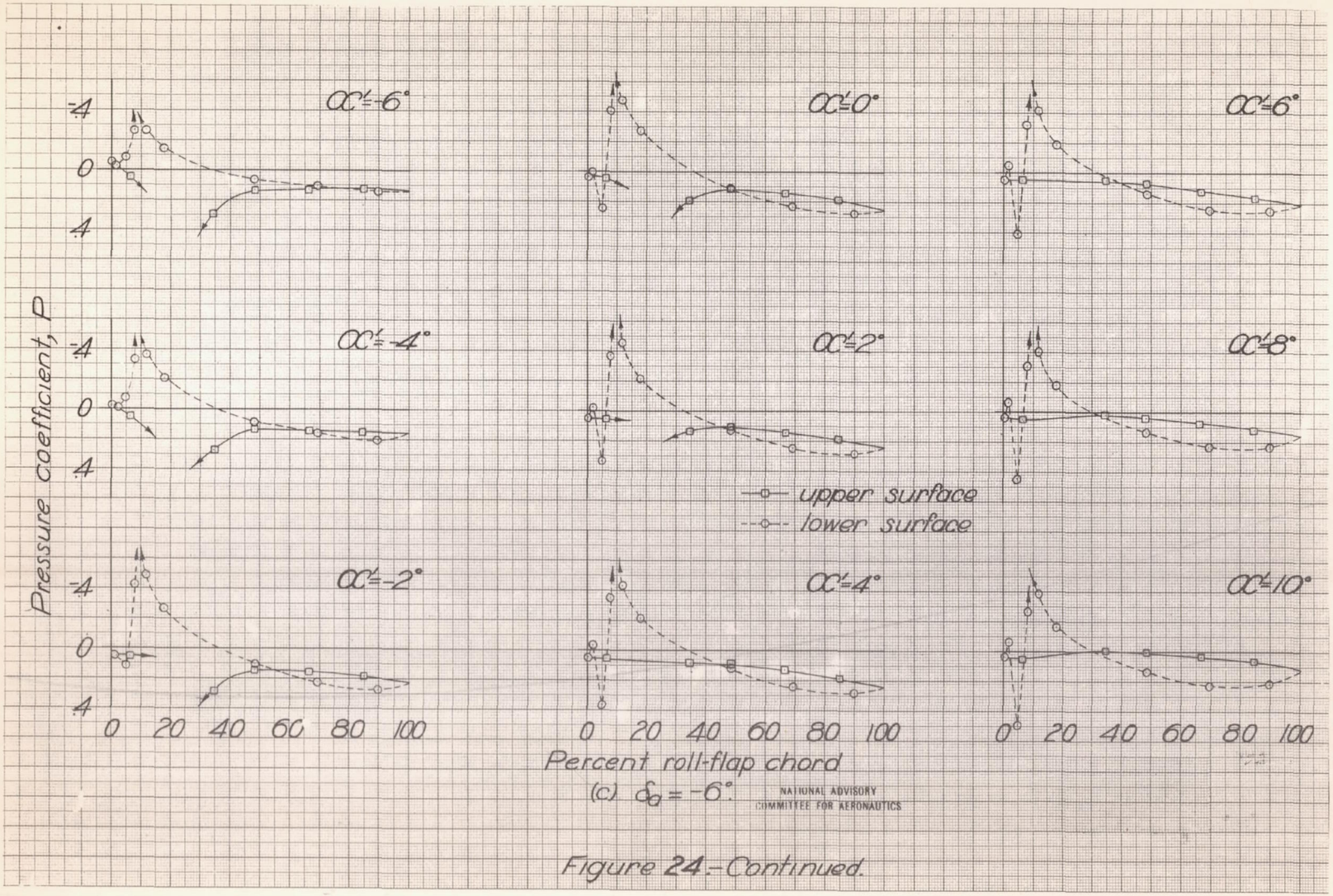

(c) $\delta_0 = -6°$.

NATIONAL ADVISORY COMMITTEE FOR AERONAUTICS

Figure 24.-Continued.

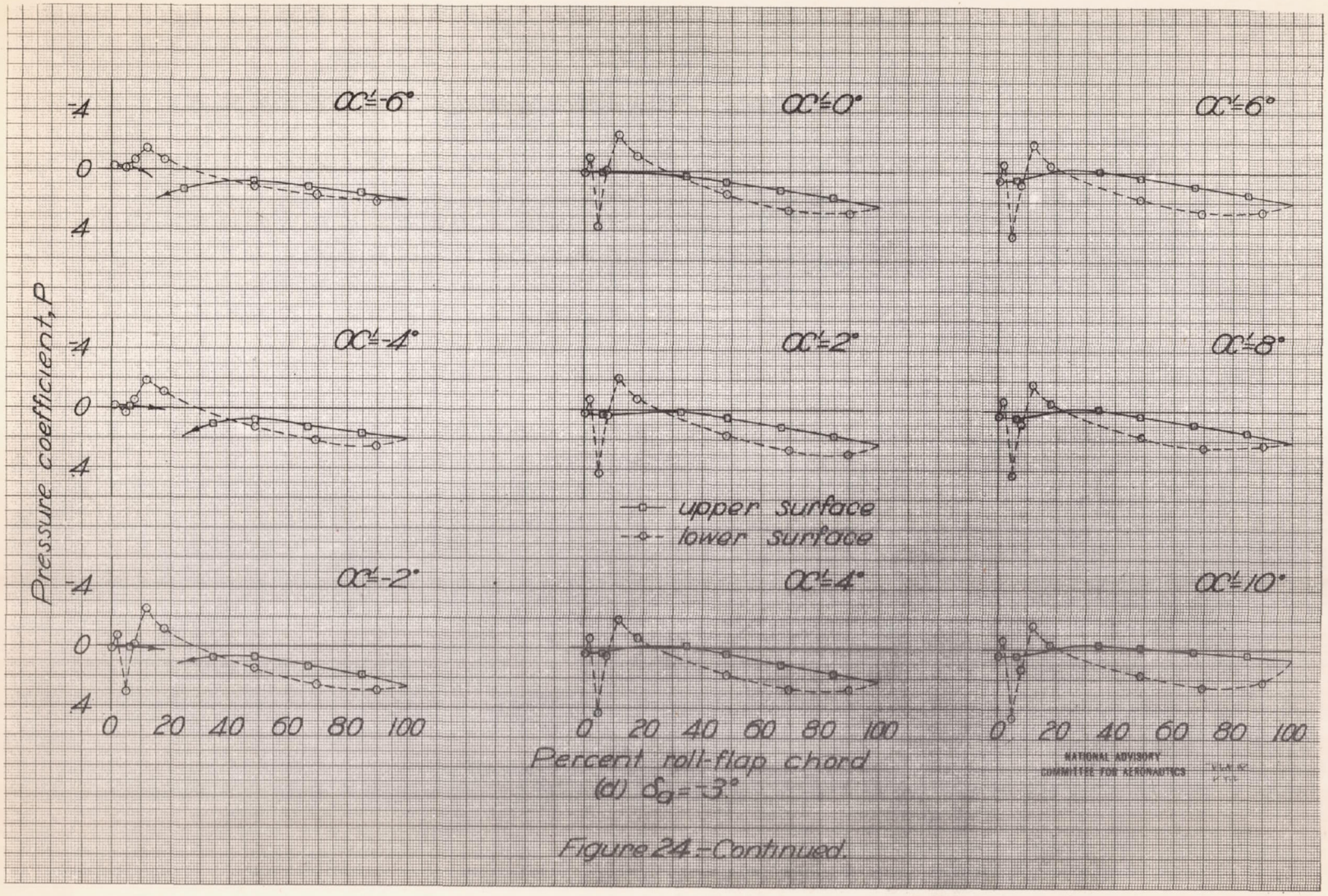

Figure 24.-Continued.

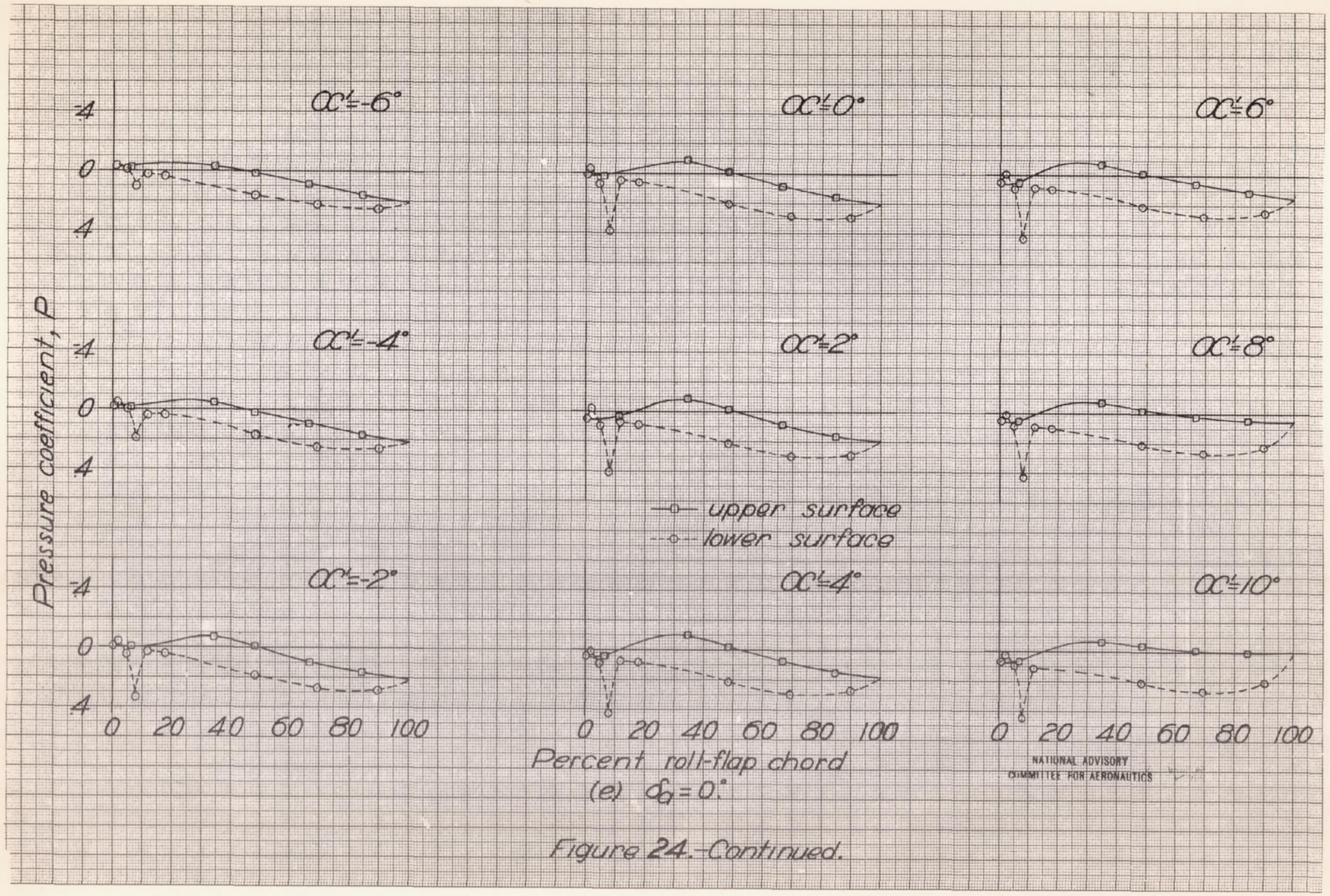

(e) $\delta_f = 0°$.

Figure 24.-Continued.

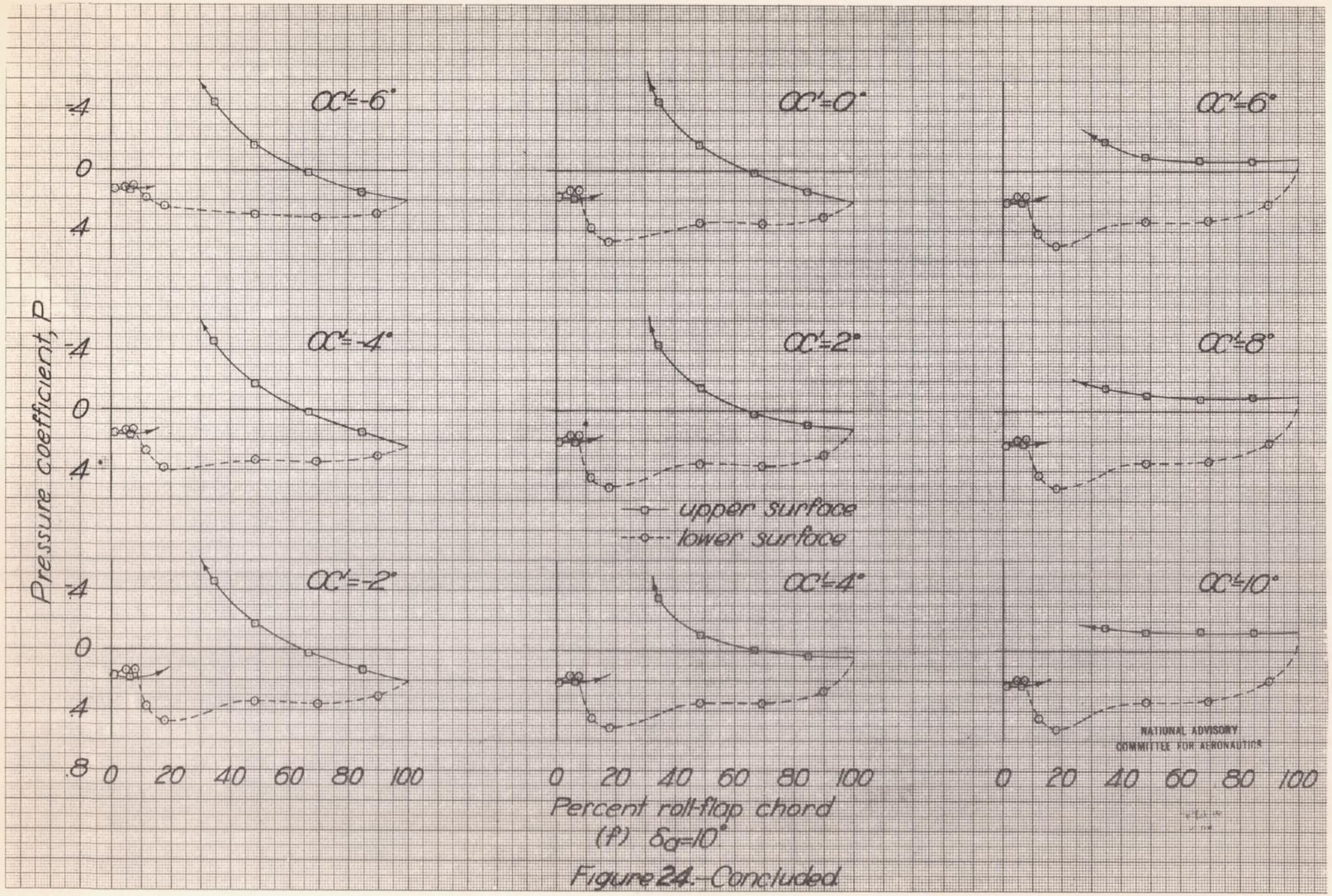

(f) $\delta_d=10°$

Figure 24.—Concluded